LA-UR-02-6420

Approved for public release; distribution is unlimited.

Title: Challenging cosmic ray propagation with antiprotons: Evidence for a ``fresh'' nuclei component?

Author(s): Igor V. Moskalenko, Andrew W. Strong, Stepan G. Mashnik, and Jonathan F. Ormes

Submitted to: The Astrophysical Journal, 586 (2003) 1050-1066; E-print: astro-ph/0210480

The Astrophysical Journal, 586:1050–1066, 2003 April 1

CHALLENGING COSMIC-RAY PROPAGATION WITH ANTIPROTONS: EVIDENCE FOR A "FRESH" NUCLEI COMPONENT?

Igor V. Moskalenko[1]
NASA Goddard Space Flight Center, Code 661, Greenbelt, MD 20771; igor.moskalenko@gsfc.nasa.gov

Andrew W. Strong
Max-Planck-Institut für extraterrestrische Physik, Postfach 1603, D-85740 Garching, Germany;
aws@mpe.mpg.de

Stepan G. Mashnik
Los Alamos National Laboratory, Los Alamos, NM 97545; mashnik@lanl.gov

and

Jonathan F. Ormes
NASA Goddard Space Flight Center, Code 600, Greenbelt, MD 20771;
Jonathan.F.Ormes@gsfc.nasa.gov
Received 2002 October 4; accepted 2002 December 2

ABSTRACT

Recent measurements of the cosmic-ray (CR) antiproton flux have been shown to challenge existing CR propagation models. It was shown that the reacceleration models designed to match secondary/primary nuclei ratios (e.g., boron/carbon) produce too few antiprotons. Matching both the secondary/primary nuclei ratio and the antiproton flux requires artificial breaks in the diffusion coefficient and the primary injection spectrum, suggesting the need for other approaches. In the present paper we discuss one possibility to overcome these difficulties. Using the measured antiproton flux *and* B/C ratio to fix the diffusion coefficient, we show that the spectra of primary nuclei as measured in the heliosphere may contain a fresh, local, "unprocessed" component at low energies, perhaps associated with the Local Bubble, thus decreasing the measured secondary/primary nuclei ratio. The independent evidence for supernova activity in the solar vicinity in the last few Myr supports this idea. The model reproduces antiprotons, B/C ratio, and elemental abundances up to Ni ($Z \leq 28$). Calculated isotopic distributions of Be and B are in perfect agreement with CR data. The abundances of three "radioactive clock" isotopes in CRs, ^{10}Be, ^{26}Al, and ^{36}Cl, are all consistent and indicate a halo size $z_h \sim 4$ kpc, based on the most accurate data taken by the *ACE* spacecraft.

Subject headings: cosmic rays — diffusion — elementary particles — Galaxy: general — ISM: general — nuclear reactions, nucleosynthesis, abundances

1. INTRODUCTION

The spectrum and origin of antiprotons in cosmic rays (CRs) have been a matter of active debate since the first reported detections in balloon flights (Golden et al. 1979; Bogomolov et al. 1979). Because of the baryonic asymmetry of the universe, antiprotons are not found at rest. There is a consensus that most of the CR antiprotons observed near the Earth are "secondaries" produced in collisions of energetic CR particles with interstellar gas (see, e.g., Mitchell et al. 1996).

The spectrum of secondary antiprotons has a peak at about 2 GeV, decreasing sharply toward lower energies. This unique shape distinguishes antiprotons from other CR species and allows for searches of primary antiprotons at low energies. Over the last few years, the accuracy has been improved sufficiently (BESS 1995–2000; Orito et al. 2000; Sanuki et al. 2000; Asaoka et al. 2002) that we can restrict the spectrum of the secondary component accurately enough to test Galactic CR propagation models and the heliospheric modulation.

It has been recently shown (Moskalenko et al. 2002) that accurate antiproton measurements during the last solar minimum, 1995–1997 (BESS; Orito et al. 2000), are inconsistent with existing propagation models at the ~40% level at about 2 GeV, while the stated measurement uncertainties in this energy range are now ~20%. The conventional models, based on local CR measurements, simple energy dependence of the diffusion coefficient, and uniform CR source spectra throughout the Galaxy, fail to reproduce simultaneously both the secondary/primary nuclei ratio and antiproton flux.

The reacceleration model designed to match secondary/primary nuclei ratios (e.g., boron/carbon) produces too few antiprotons because, e.g., matching the B/C ratio at all energies requires the diffusion coefficient to be too large. The models without reacceleration can reproduce the antiproton flux; however, they fall short of explaining the low-energy decrease in the secondary/primary nuclei ratio. To be consistent with both, the introduction of breaks in the diffusion coefficient and the injection spectrum is required, which would suggest new phenomena in particle acceleration and propagation.

Recently there has appeared some indication that the atmospheric contribution to the antiproton flux measured in the upper atmosphere is underestimated. If this is true, the reacceleration model could still be the best one to describe propagation of nucleon species in the Galaxy (for more details, see § 8). However, in this work we have assumed that

[1] Also Joint Center for Astrophysics, University of Maryland, Baltimore County, Baltimore, MD 21250.

the published Galactic antiproton flux, corrected for atmospheric production, is accurate.

In the present paper we discuss another possibility to overcome the difficulties encountered by reacceleration models. We show that the inclusion of a local primary component at low energies, perhaps associated with the Local Bubble (LB), reconciles the data.

2. INTERSTELLAR COSMIC-RAY SPECTRUM

Just as secondary nuclei, the product of the disintegration of primary nuclei, are abundant in CRs but rare in the interstellar medium (ISM), diffuse γ-rays, antiprotons, and positrons are secondary products of interactions of mostly CR protons and helium nuclei with interstellar gas. The CR propagation model that describes any secondary/primary ratio should equally well describe all the others: B/C, sub-Fe/Fe, and $\bar{p}/p$ ratios and spectra of nuclei, positrons, and diffuse Galactic continuum γ-rays.

The diffusive reacceleration models naturally reproduce secondary/primary nuclei ratios in CRs and agree better with K-capture parent/daughter nuclei ratio (see, e.g., Jones et al. 2001a), although this result is not completely conclusive because of the large error bars in CR measurements and uncertainties in important isotopic cross sections. It is, however, clear that some reacceleration is unavoidable in the ISM. Because of the unique shape of the antiproton spectrum, reacceleration has a much weaker effect on it than in the case of nuclei. Taking into account that the antiproton production spectrum can be calculated accurately, antiprotons provide a unique complementary tool to test propagation models (and heliospheric modulation).

Our previous result (Moskalenko et al. 2001b, 2002), in agreement with calculations of other authors (Molnar & Simon 2001), was that matching the secondary/primary nuclei ratio B/C using reacceleration models leads to values of the spatial diffusion coefficient apparently too large to produce the required antiproton flux, when the propagated nucleon spectra are tuned to match the local proton and helium flux measurements. This is an essential shortcoming.

Assuming that the measured antiproton flux is correct and the current heliospheric modulation models are approximately right, we have the following possibility to reconcile the B/C ratio with the required flux of secondary antiprotons. The spectra of primary nuclei as measured in the heliosphere may contain a fresh, local, "unprocessed" component at low energies, thus decreasing the measured secondary/primary nuclei ratio. This component would have to be local in the sense of being specific to the solar neighborhood, so that the well-known Local Bubble phenomenon is a natural candidate.

The idea that CRs are accelerated out of supernova (SN) ejecta–enriched matter in superbubbles has been discussed in numerous papers (see, e.g., Higdon, Lingenfelter, & Ramaty 1998 and references therein). The possibility that the "fresh" component is coming from the LB has been discussed by, e.g., Morfill & Freyberg (1998) and Davis et al. (2000). We hereafter call it the "LB hypothesis." The idea is that primary CRs like ^{12}C and ^{16}O have a local component at low energies, while secondary CRs like B are produced Galaxy-wide over the confinement time of 10–100 Myr. Then the B/C ratio will be lower at low energies than expected in a uniform model, because of the enhanced local C (and the reduced Galactic production of B). If this idea is correct, then the high-energy part of the secondary/primary nuclei ratio plus the measured antiproton flux at maximum, $\sim$2 GeV, can be used to restrict the value and energy dependence of the diffusion coefficient, while the required contribution of the local sources can be derived from the measured secondary/primary nuclei ratio at low energies.

One additional hint for the possible existence of an unprocessed component is the calculated ratio $^{13}\mathrm{C}/^{12}\mathrm{C} \sim 0.14$ at 120 MeV nucleon^{-1} (modulation potential 500 MV), which appears to be a factor of 2 larger than that observed when the propagation parameters are tuned to the B/C ratio (Moskalenko et al. 2002). The isotope ^{13}C is almost all secondary, as are Be and B isotopes. Since the primary source of ^{13}C is ^{16}O, accounting for as much as $\sim$60% of the total, this may indicate an "overenrichment" of the assumed source abundances in oxygen. If so, the overenrichment may be true also for primary carbon, but tuning to the observed B/C artificially eliminates the excess of lithium, beryllium, and boron. We note that the ratio $^{15}\mathrm{N}/^{16}\mathrm{O}$ is, however, correct, and the problem with overproduction of ^{13}C may arise from cross section errors (see the Appendix).[2]

3. THE LB HYPOTHESIS

The low-density region around the Sun, filled with hot H I gas, is called the Local Bubble (see, e.g., Sfeir et al. 1999). The size of the region is about 200 pc, and it is likely that it was produced in a series of SN explosions. Most probably its progenitor was an OB star association. Although people discuss different scenarios (see, e.g., Maíz-Apellániz 2001; Berghöfer & Breitschwerdt 2002), the LB age and the number of SN progenitors appear to be similar, $\sim$10 Myr and $\sim$10–20 SNs, respectively. Most probably they exploded as core-collapse SNs II or thermonuclear SNs Ib/c with a mass of pre-SN stars between several and $\sim$10 $M_{\odot}$, with the last SN explosion occurring approximately 1–2 Myr ago, or three SNs occurring within the last 5 Myr.

There is also some evidence of an SN explosion nearby. An excess of ^{60}Fe measured in a deep ocean core sample of ferromanganese crust suggests the deposition of SN-produced iron on Earth (Knie et al. 1999). The enhanced concentrations were found in two of three layers corresponding to a time span of less than 2.8 Myr and 3.7–5.9 Myr, respectively. The study suggests an SN explosion about 5 Myr ago at 30 pc distance. Another study reports an enhancement in the CR intensity dated about 40 kyr ago (Sonett, Morfill, & Jokipii 1987), which is interpreted as the passage across the solar system of the shock wave from an SN exploding about 0.1 Myr ago. Taking into account possible errors of all these estimates, they point to a nearby SN explosion some 1 Myr ago (see also discussion in Benítez, Maíz-Apellániz, & Canelles 2002).

It could also be that fresh LB contributions from continuous acceleration in the form of shock waves (Bykov & Fleishman 1992) and/or energetic particles coming directly from SN remnants still influence the spectra and abundances of local CRs. The elemental abundances of the low-energy nonthermal component in a superbubble can differ strongly from the standard cosmic abundances (Bykov

[2] The production cross sections of ^{14}N and ^{15}N and of ^{12}C and ^{13}C have been measured only in a narrow energy range.

2001) because of ejection of matter enriched with heavy elements from SNe and stellar winds of massive stars (Wolf-Rayet, OB stars). The continuous acceleration is connected with the lifetime of a shock wave in the LB. A reasonable estimate is given by the sound crossing time, approximately 2 Myr, for a distance of 200 pc in a 10^6 K plasma (Berghöfer & Breitschwerdt 2002). On the other hand, the particle crossing time can be estimated as $t \sim x^2/D \sim 1$ Myr for a typical value of the diffusion coefficient in the ISM $D \sim 10^{28}$ cm s^{-2} and $x \sim 200$ pc. Therefore, accelerated particles are expected to be present in this region.

4. THE CALCULATION PROCEDURE

In our calculations we use the propagation model GALPROP[3] as described elsewhere (Strong & Moskalenko 1998; Moskalenko et al. 2002); for the present purpose the two-dimensional, cylindrically symmetrical option is sufficient. For a given halo height z_h the diffusion coefficient as a function of momentum and the reacceleration or convection parameters is determined by data on secondary/primary ratios in CRs. The spatial diffusion coefficient is taken as $D_{xx} = \beta D_0 (\rho/\rho_0)^{\delta}$; the corresponding diffusion in momentum space and other details of the models can be found in our earlier papers. We use our standard methodologies and include two types of CR sources. Antiproton production and propagation are calculated as described in Moskalenko et al. (2002).

The nucleon injection spectrum of the Galactic component was taken as a modified power law in rigidity (Jones et al. 2001b), $dq(p)/d\rho \propto \rho^{-\gamma}/[1 + (\rho/2)^{-2}]^{1/2}$, for the injected particle density. The proton and He spectra are tuned to the local measurements as described in Moskalenko et al. (2002).

The LB spectrum is taken to have the form (as suggested by Bykov & Fleishman 1992 and Bykov 2001 for continuous acceleration by interstellar shocks) $df/d\rho \propto \rho^{-\eta} \exp(-\rho/\rho_b)$, where ρ is the rigidity and ρ_b is the cutoff rigidity. The LB source abundances and ρ_b are adjustable parameters. In terms of kinetic energy per nucleon E, this can be rewritten as

$$\frac{df}{dE} = a(Z, A)\,\frac{A(E+m)}{Zp}\,\rho^{-\eta}\exp(-\rho/\rho_b)\ , \qquad (1)$$

where $a(Z, A)$ is the abundance of a nucleus (Z, A), Z and A are the nucleus charge and atomic number, respectively, m is the atomic mass unit, p is the momentum per nucleon, and $\rho_b = (A/Z)[(E_b + m)^2 - m^2]^{1/2}$. The particular spectral shape of the LB component is not important as long as it decreases sharply toward high energies and is much softer than the Galactic CR spectrum. We show the results obtained with $\eta = 1$, but they are very similar with $\eta = 2$, with ρ_b adjusted correspondingly.

The procedure to tune the CR elemental abundances, secondary/primary nuclei ratios, and antiproton flux we adopted was as follows. The high-energy parts of B/C ratio and antiproton flux measurements are used to restrict the value of the diffusion coefficient and its energy dependence, while the low-energy part of the B/C ratio is used to fix a value for the reacceleration level and define the parameters of the LB component.

The heliospheric modulation is treated using the force field approximation (Gleeson & Axford 1968). In our previous paper (Moskalenko et al. 2002), we used the best currently available model of the heliospheric modulation, the steady state drift model. The use of the simpler model in the current paper is justified by the following arguments. First, in the previous paper (Moskalenko et al. 2002) we tried to build a model of particle propagation explaining both CR nuclei and antiproton fluxes equally well. The heliospheric modulation calculation was considered one of the main possible reasons for the discrepancy between the nuclei and antiproton fluxes. It appears, however, that the interstellar propagation and/or cross section errors are responsible for the nuclei/antiproton discrepancy, unless the current models of heliospheric modulation are *completely* wrong, which is not very likely. Second, the current paper evaluates a new hypothesis for the origin of CRs, in which the main emphasis is on the local CR component. Use of a sophisticated modulation model containing additional unknown variables will make such evaluation unnecessarily complicated. Third, the parameters of the diffusion coefficient are fixed using the data above few GeV, for which the modulation is weak.

We consider three different models (Table 1), with parameters fixed using the described procedure. They are the simplest plain diffusion model (PD) and two reacceleration models, which use different assumed isotopic abundances in the Galactic CR and LB sources. Diffusive reacceleration model I (DR I) has the same isotopic abundances in Galactic CR and LB sources. Diffusive reacceleration model II (DR II) is the same as DR I, except that the LB isotopic abundances are tuned to match the low-energy data from

[3] The GALPROP model, including software and data sets, is available at http://www.gamma.mpe-garching.mpg.de/~aws/aws.html.

TABLE 1
PROPAGATION PARAMETER SETS

MODEL	INJECTION INDEX (γ)	DIFFUSION COEFFICIENT[a]		ALFVÉN SPEED[b]	SOURCE ABUNDANCES
		D_0 (cm^2 s^{-1})	INDEX (δ)	(km s^{-1})	
Plain diffusion (PD).....	2.16	3.10×10^{28}	0.60	...	...
Diffusive reacceleration I (DR I)	2.28	3.30×10^{28}	0.47	23	LBS = CRS
Diffusive reacceleration II (DR II).....	2.28	3.30×10^{28}	0.47	23	LBS $\neq$ CRS

NOTE.—Adopted halo size $z_h = 4$ kpc.
[a] $\rho_0 = 3$ GV.
[b] $v_A/w^{1/2}$, where v_A is the Alfvén speed and w is defined as the ratio of MHD wave energy density to magnetic field energy density.

ACE and *Ulysses*, thus increasing the freedom to fit the data. The Galactic CR elemental source abundances (DR II model) are tuned to the abundances measured at high energies, at which the heliospheric modulation is weak.

The PD model, without an LB component, has already been discussed in Moskalenko et al. (2002). It is inconsistent with low-energy data on secondary/primary ratios, and at high energies matching the B/C ratio would cause an overproduction of antiprotons. We do not see a plausible modification of this model, even including an LB component, that would allow to us simultaneously fit antiprotons and the B/C ratio.

Hence, we turn to the models with reacceleration. Figure 1*a* illustrates the process of fixing the normalization of the diffusion coefficient using antiprotons. The antiproton flux is shown as calculated in the DR I and II models with $\delta = 0.47$ and different normalizations in the diffusion coefficient, $D_0 = 2.6 \times 10^{28}$, 3.3×10^{28}, and 4.3×10^{28} cm s^{-2} at $\rho = 3$ GV (for antiprotons this corresponds to kinetic energy $\sim$2 GeV). The injection index γ is taken to be equal to 2.28, and the Alfvén speed $v_A = 23$ km s^{-1}. The antiproton flux at maximum, $\sim$2 GeV, appears to be quite sensitive to the value of the diffusion coefficient and allows us to fix it at $D_0 = (3.3 \pm 0.8) \times 10^{28}$ cm s^{-2}. (A 1 σ deviation in the data translates to approximately $^{+25\%}_{-20\%}$ accuracy in D_0.) The exact value of δ is not critical, since we compare with the antiproton measurements at maximum, $\sim$2 GeV. Inelastically scattered antiprotons, the "tertiary" component, appear to be important at low energies only in the ISM. Figure 1*b* shows corresponding calculations of the B/C ratio. A halo height of $z_h = 4$ kpc is used (Strong & Moskalenko 2001; Moskalenko, Mashnik, & Strong 2001a). Using values differing by up to a factor of 2 (the estimated uncertainty) would not affect the conclusions; the diffusion coefficient would simply scale accordingly: $D_0 \propto z_h$, approximately. In § 6.2, we reevaluate the radioactive secondaries for the current model and show that our adopted value of z_h is in good agreement with the data.

The LIS proton and helium spectra used in our antiproton calculations are the best fits to the data, as described in Moskalenko et al. (2002). The proton spectrum is shown in Figure 2, together with data. Because of the measurements with large statistics, mostly by BESS (Sanuki et al. 2000) and AMS (Alcaraz et al. 2000), and weak heliospheric modulation above 10 GeV, the error arising from uncertainties in the primary spectra is only $\sim$5%. The agreement between BESS and AMS data, currently considered to be the most accurate, is impressive. The data collected by other instruments (IMAX, CAPRICE, and LEAP) at approximately the same solar modulation level are lower by 5%–10% and have larger error bars. Adopting a smaller LIS proton flux would lead to an even more dramatic discrepancy between the antiproton flux data and the calculation in the "standard" reacceleration model (Moskalenko et al. 2002). In any case, allowing for a $\sim$5%–10% systematic uncertainty in the proton measurements does not change the conclusions of the present paper, because the antiproton data have larger error bars.

We note that as in the case of other nuclei, there should be an LB contribution to proton and He spectra. The Galactic injection spectra of protons and He should thus be significantly flatter below several GeV, to match the data points at low energies. This does not influence the antiproton production, because (1) the LB does not produce a significant

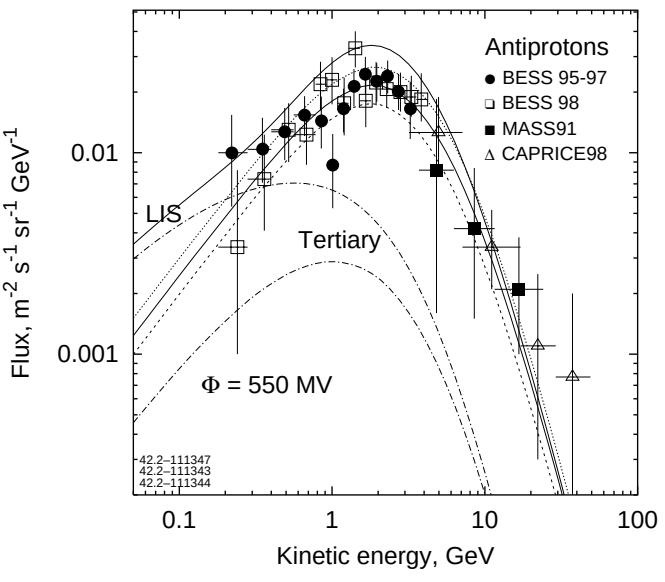

FIG. 1*a*

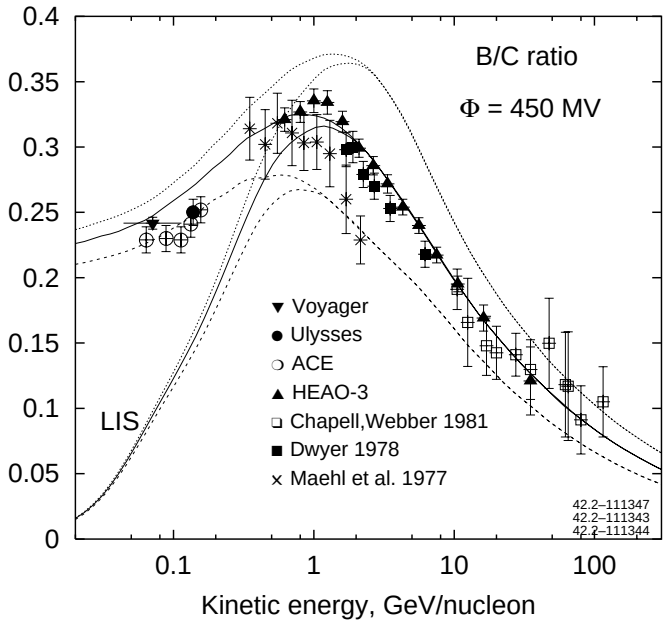

FIG. 1*b*

FIG. 1.—(*a*) Antiproton flux calculated in DR I/II models with index $\delta = 0.47$ in the diffusion coefficient and different normalization values D_0. *Solid curves*: $D_0 = 3.3 \times 10^{28}$ cm s^{-2} at $\rho_0 = 3$ GV; *upper curve*, local interstellar (LIS); *lower curve*, modulated. *Dotted curve*: $D_0 = 2.6 \times 10^{28}$ cm s^{-2} (modulated). *Dashed curve*: $D_0 = 4.3 \times 10^{28}$ cm s^{-2} (modulated). The dash-dotted curves show the LIS spectrum and modulated tertiary component, respectively, for $D_0 = 3.3 \times 10^{28}$ cm s^{-2}. Modulation was made with $\Phi = 550$ MV (force field). Data: BESS 1995–1997 (Orito et al. 2000), BESS 1998 (Asaoka et al. 2002), MASS91 (Basini et al. 1999), and CAPRICE98 (Boezio et al. 2001). (*b*) B/C ratio calculated with LB contribution, $E_b = 500$ MeV. Curves are coded as in (*a*), with lower curves for LIS and upper curves modulated ($\Phi = 450$ MV). Data below 200 MeV nucleon^{-1}: *ACE* (Davis et al. 2000), *Ulysses* (DuVernois, Simpson, & Thayer 1996), and *Voyager* (Lukasiak, McDonald, & Webber 1999). High-energy data: *HEAO 3* (Engelmann et al. 1990). For other references, see Stephens & Streitmatter (1998).

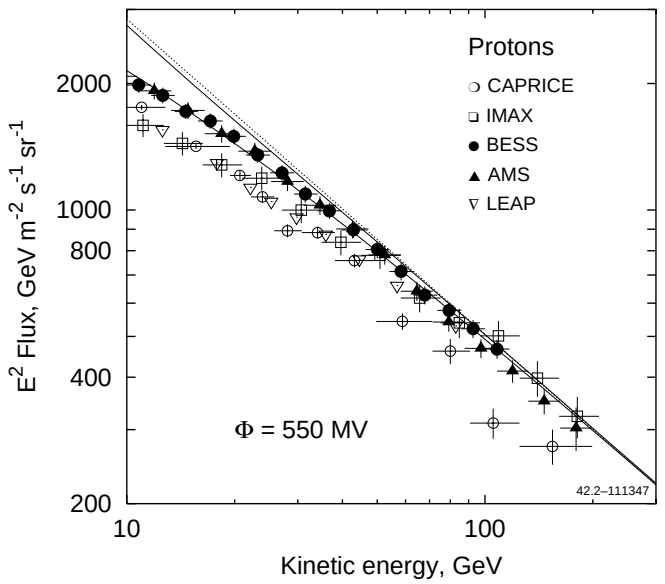

FIG. 2.—Proton spectrum as calculated in DR I/II models, compared with the data. *Upper curve*: LIS; *lower curve*: modulated to 550 MV. The dotted line shows the LIS spectrum best fitted to the data above 20 GeV (Moskalenko et al. 2002). Data: IMAX (Menn et al. 2000), CAPRICE (Boezio et al. 1999), BESS (Sanuki et al. 2000), AMS (Alcaraz et al. 2000), and LEAP (Seo et al. 1991).

amount of secondaries and (2) the antiproton threshold production energy is high, ~10 GeV.

Further tuning can be done using the high-energy part of the B/C ratio, which is not influenced by heliospheric modulation and supposedly contains only a Galactic component of CRs. Figure 3*a* shows a calculation of the B/C ratio for $E_b = 500$ MeV and different energy dependencies of the diffusion coefficient. The plotted curves correspond to values of the power-law index $\delta = 0.42$, 0.47, and 0.52, while the injection index was tuned to match the high-energy spectral data. Index $\delta \sim 0.47$ is chosen as giving the best match. A pure Kolmogorov spectrum, $\delta = \frac{1}{3}$, thus seems to be excluded by antiproton spectrum data taken in combination with B/C ratio data.

The B/C ratio as calculated with and without a contribution of the LB component is shown in Figure 3*b*. The LB component is shown calculated with $E_b = 400$, 500, and 600 MeV. It is seen, however, that all three provide good agreement with B/C data. Figure 4 shows the interstellar and LB carbon spectra in this model. By including the LB component, we have therefore been able to obtain a model simultaneously fitting p, He, $\bar{p}$, and B/C data. It now remains to apply this model to the full range of CR isotopes.

4.1. *Calculation Uncertainties*

We do not discuss here possible calculation *errors*. Derivation of such errors is a *very* complicated matter, given the many uncertainties in the input, such as the cross sections, gas distribution in the Galaxy, systematic errors in the CR measurements, heliospheric modulation, and atmospheric corrections. Some possible errors and their effects have been discussed in Moskalenko et al. (2002). Here we qualitatively mention what we think may affect our conclusions and what may not.

Possible errors in the cross section of the abundant CR nuclei seem to be less important, as they can be compensated for by relatively small corresponding adjustments in the primary abundances. They may, however, be more important in case of less abundant secondary nuclei. The cross section errors are extensively discussed throughout this paper.

Errors in the Galactic gas distribution are not so important in the case of stable and long-lived nuclei. Such errors

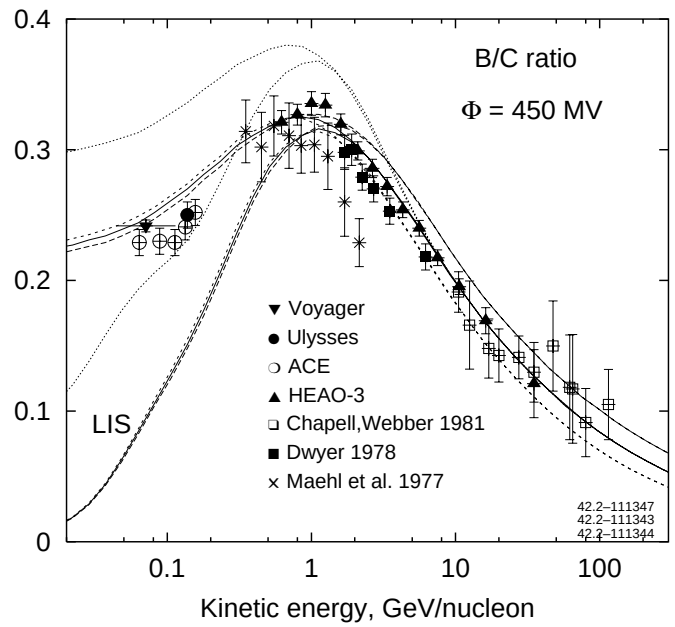

FIG. 3*a*

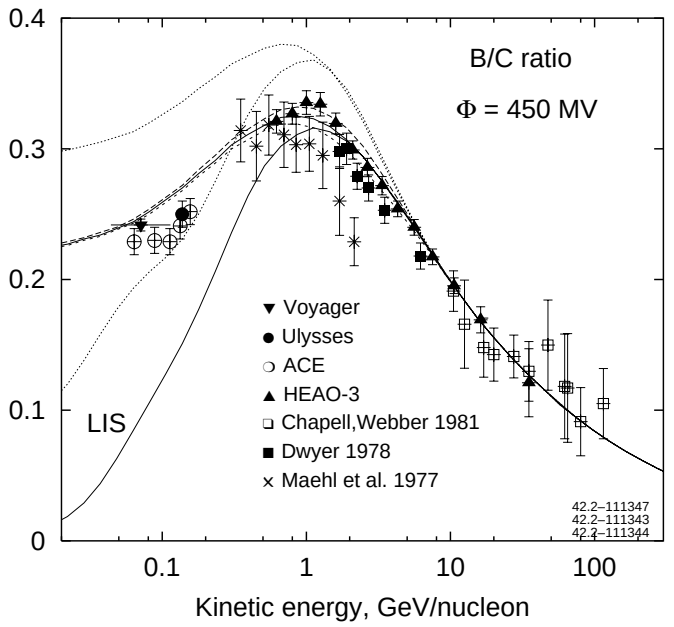

FIG. 3*b*

FIG. 3.—B/C ratio calculated without (*dotted curves*) and with (*all other curves*) LB contribution (DR I/II models). (*a*) $E_b = 500$ MeV, with energy dependence in the diffusion coefficient $\delta = 0.52$ (*short-dashed curves*), 0.47 (*solid curves*), and 0.42 (*long-dashed curves*), with lower curves for LIS and upper curves modulated ($\Phi = 450$ MV). Data as in Fig. 1*b*. (*b*) $E_b = 400$ (*long-dashed curves*), 500 (*solid curves*), and 600 MeV (*short-dashed curves*). Lower and upper curves and data as in (*a*).

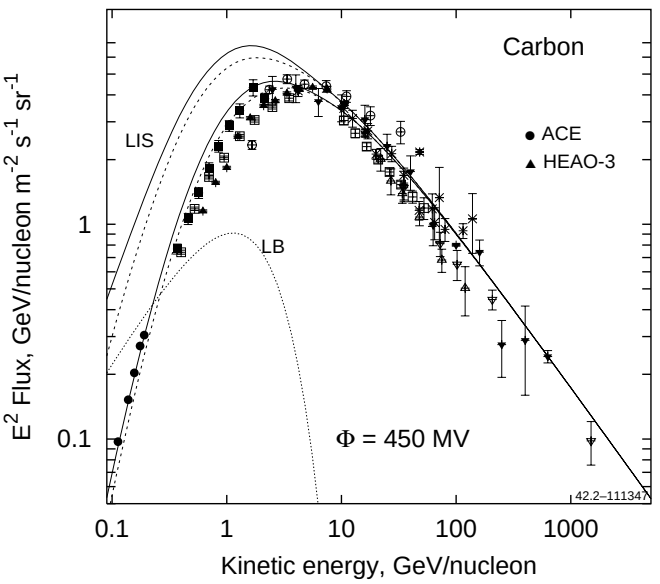

FIG. 4.—Spectrum of carbon calculated with (*solid curves*; DR II model) and without (*dashed curves*) LB contribution. *Upper curves*: LIS; *lower curves*: modulated using force field approximation ($\Phi = 450$ MV). LB interstellar spectrum is shown as a dotted curve. Data: *ACE* (Davis et al. 2000, 2001) and *HEAO 3* (Engelmann et al. 1990). For other references see Stephens & Streitmatter (1998) (symbols are changed).

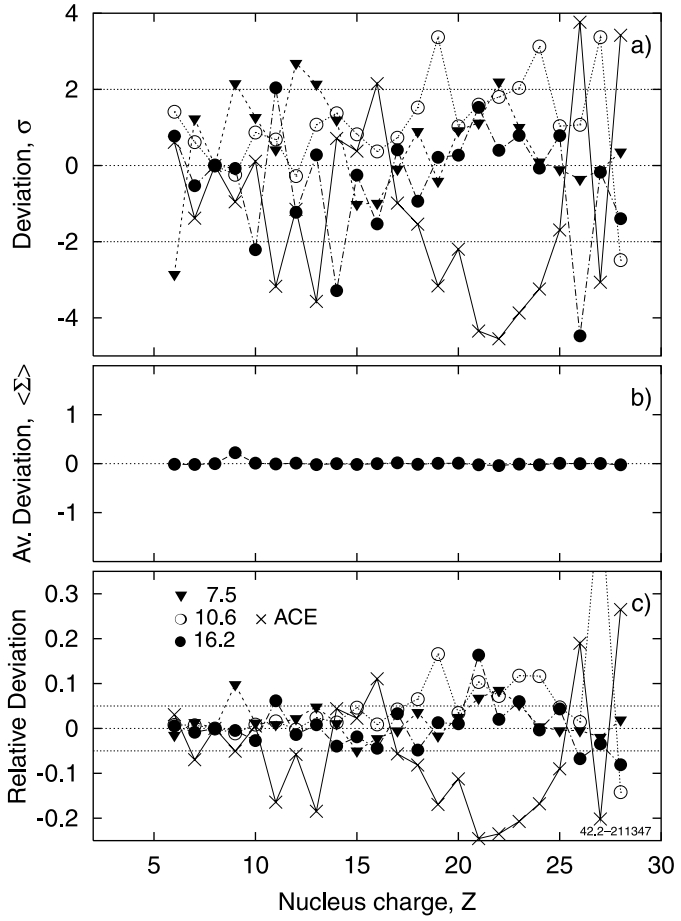

FIG. 5.—Deviation of propagated abundances (DR I model) from those measured by *HEAO 3* at 7.5, 10.6, and 16.2 GeV nucleon^{-1} (Engelmann et al. 1990) and *ACE* at 200 MeV nucleon^{-1} (Wiedenbeck et al. 2001) (*a*) separately for each energy in σ's, (*b*) averaged for four energies in σ's, and (*c*) relative.

are compensated for simultaneously for all species by the corresponding adjustment of the propagation parameters (diffusion coefficient).

Heliospheric modulation may introduce some error, but it will be similar for all CR nuclei (or their ratios) because the critical parameter here is the charge/mass ratio, approximately $\frac{1}{2}$ for all nuclei except (anti)protons.

Systematic measurement errors are difficult to account for, but their effect can be reduced by careful choice of the data to rely on. This is what we try to do in the present paper.

Such an effect as the atmospheric correction to the observed antiproton flux is very important and may affect our results. We discuss it in more detail in § 8.

5. APPLICATION TO NUCLEI UP TO Ni

The DR I model gives an approximate fit to all elements (Fig. 5). The source elemental abundances are tuned (at a nominal reference energy of 100 GeV), by a least-squares procedure, to the abundances measured by *HEAO 3* (Engelmann et al. 1990) at 7.5, 10.6, and 16.2 GeV nucleon^{-1} combined with *ACE* 200 MeV nucleon^{-1} data, assuming modulation potential $\Phi = 400$ MV. At the chosen *HEAO 3* energies the heliospheric modulation is weak (for the epoch 1980 we adopt $\Phi = 800$ MV), and it is in the middle of the logarithmic interval 0.6–35 GeV nucleon^{-1} covered by the *HEAO 3* measurements; thus, the systematic and statistical errors are minimal. To the statistical errors of the *ACE* data we added 5% systematic error, which is a minimal, conservative estimate of the uncertainties in the measurements and modulation potential.

Figure 5 shows the quality of the fit. Figure 5*a* shows the deviation of the calculated abundances from measurements at a given energy expressed in standard deviations. Figure 5*b* shows the average deviation $\langle\Sigma\rangle = (1/n)\sum_{i=1}^{n}[(A_i^t - A_i^m)/\sigma_i]$, where A_i^t, A_i^m are the calculated and measured abundances for the given energy and σ_i is the standard deviation. Figure 5*c* shows the relative deviation of the calculated abundances from measurements at a given energy.

The DR I fit is systematically low[4] at low energies (*ACE*), by as much as 15%–30% for elements with $Z = 11$, 13, and 19–25. It disagrees with high-energy abundance of iron by ~20% and by more than 50% with that of $_{27}$Co and $_{28}$Ni. Meanwhile, the high-energy data taken separately are consistent within 5%–10% (Fig. 5*c*). Because of this low-energy discrepancy, we consider further only the DR II model, in which we allow Galactic CR and LB abundances to be different. In this model, the low-energy data are used to determine the LB source abundances. The DR II model provides the best fit to all data at the cost of extra free parameters.

In the DR II model, the Galactic CR source elemental abundances are tuned (at a nominal reference energy of 100 GeV), by a least-squares procedure, to the abundances measured by *HEAO 3* (Engelmann et al. 1990) at 5.6, 7.5, 10.6, and 16.2 GeV nucleon^{-1} (Fig. 6). Figure 7 shows calculated propagated abundances versus *HEAO 3* data at one

[4] This may be due to the errors in the production cross sections employed in the calculations.

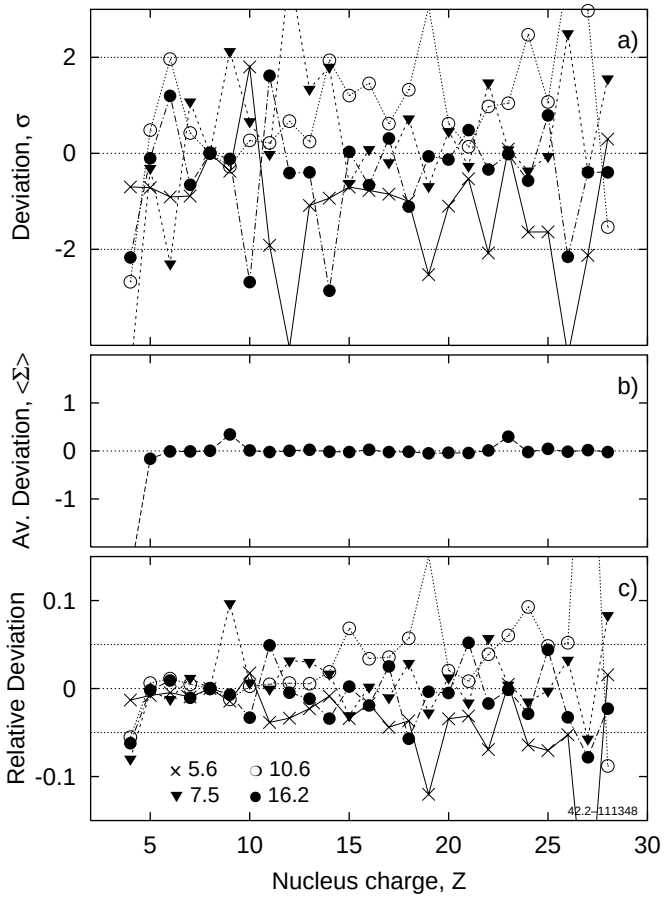

FIG. 6.—Deviation of propagated abundances (DR II model) from those measured by *HEAO 3* at 4.3, 5.6, 7.5, 10.6, and 16.2 GeV nucleon^{-1} (Engelmann et al. 1990) (*a*) separately for each energy in σ's, (*b*) averaged for all five energies in σ's, and (*c*) relative.

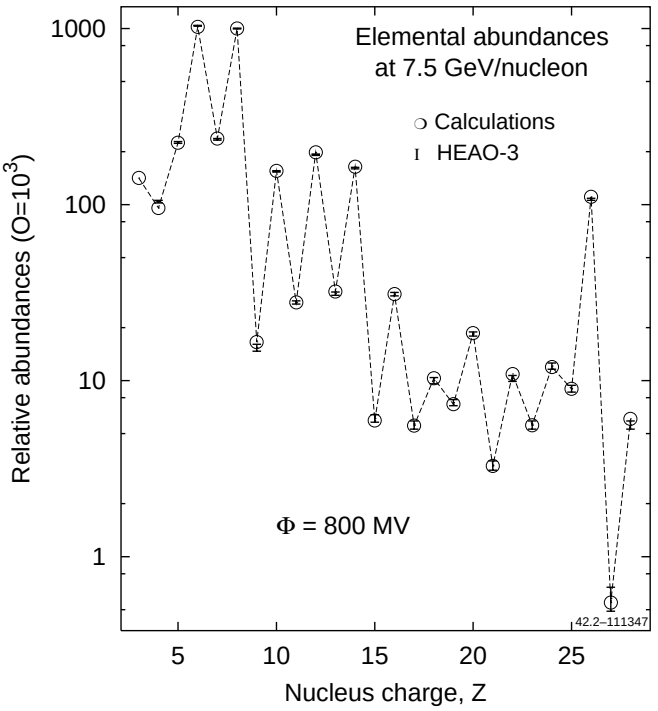

FIG. 7.—Calculated propagated elemental abundances at 7.5 GeV nucleon^{-1} (DR II model). Modulation uses force field approximation ($\Phi = 800$ MV). Data: *HEAO 3* (Engelmann et al. 1990).

particular energy, 7.5 GeV nucleon^{-1}. Relative isotopic abundances at the source are taken equal to solar system abundances (Anders & Grevesse 1989). The key point in the fitting procedure is to obtain the correct abundance of boron.

Figure 6 shows the quality of the fit to high-energy data, where Figures 6*a*, 6*b*, and 6*c* show the deviation of the calculated abundances from measurements at a particular energy expressed in standard deviations, an average deviation, and the relative deviation of the calculated abundances from measurements at a given energy, respectively. The deviations from the data at any particular energy are almost all within ~5%. The calculated abundance of $_4$Be appears to be ~7% below that from the *HEAO 3* data. It is, however, the lightest nucleus measured by the apparatus, and its measurements thus may be affected by systematic errors. Some disagreement in calculated and measured abundances of $_9$F and $_{23}$V, as seen in Figure 6*b*, is caused by overproduction at only one energy point, 7.5 GeV nucleon^{-1} in case of $_9$F and 10.6 GeV nucleon^{-1} in case of $_{23}$V, while at other energies calculations agree well with data. Ten percent overproduction of $_{24}$Cr is seen only at one energy, 10.6 GeV nucleon^{-1}. Compared to the calculations, measurements of $_{19}$K and $_{27}$Co are particularly scattered; $_{27}$Co is the least abundant element for $Z < 29$, and its abundance in CRs is measured with large error bars. $_{28}$Ni is at the end of the nucleus charge interval measured by *HEAO 3*, and probably its measurement is also affected by the systematic errors. In general, the deviations in measurements are larger for the least abundant nuclei, which is not surprising.

The LB elemental abundances are tuned simultaneously with spectra using the low-energy part of the B/C ratio and isotopic abundances at 200 MeV nucleon^{-1} from *ACE* (Wiedenbeck et al. 2001) and at 185 MeV nucleon^{-1} from *Ulysses* (DuVernois & Thayer 1996). For many elements *ACE* and *Ulysses* abundances differ by 10% (Fig. 8*c*). For this reason, to the statistical errors shown we added 5% systematic error. In the same way as for the high-energy data, Figure 8 shows the quality of the fit to low-energy data by *ACE* and *Ulysses*.

The fitting procedure is also influenced by the adopted value of the modulation potential. We found that applying the following pairs of modulation potentials yields almost the same LB elemental abundances: 400 MV for *ACE* and 700 MV for *Ulysses*, 450 MV for *ACE* and 600 MV for *Ulysses*, and 500 MV for *ACE* and 500 MV for *Ulysses*. Other combinations of modulation potentials make the quality of the fit worse. The data are shown to deviate from calculations in both directions, which means that we are unlikely to introduce essential systematic error by assuming a wrong value of the modulation potential.

6. ABUNDANCES IN COSMIC RAYS AND COSMIC-RAY SOURCES

6.1. *Elemental Abundances in Cosmic-Ray Sources*

The DR II model with an LB component shows good overall agreement with data, including secondary/primary ratios, spectra, and abundances. The derived Galactic CR source abundances and LB source abundances are given in Table 2 and plotted in Figure 9 relative to the solar system

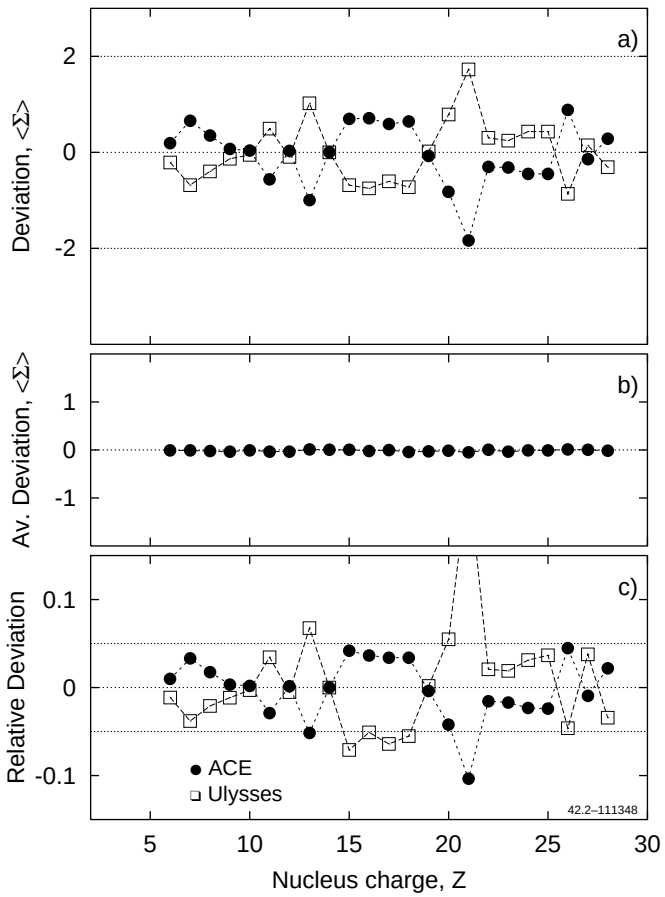

FIG. 8.—Deviation of propagated abundances (DR II model) from those measured by *ACE* (Wiedenbeck et al. 2001) and *Ulysses* (DuVernois & Thayer 1996) (*a*) separately for each energy in σ's, (*b*) averaged for both sets of data in σ's, and (*c*) relative.

TABLE 2
ELEMENTAL ABUNDANCES

Z	Solar System	LB Sources[a]	Galactic Sources
6.....	9.324	3.850	4.081
7.....	2.344	6.500×10^{-1}	3.022×10^{-1}
8.....	19.04	6.317	5.235
9.....	8.901×10^{-4}	0.0	0.0
10.....	3.380	6.667×10^{-1}	6.328×10^{-1}
11.....	6.028×10^{-2}	9.767×10^{-2}	3.575×10^{-2}
12.....	1.070	1.385	1.050
13.....	8.310×10^{-2}	1.583×10^{-1}	7.794×10^{-2}
14.....	1.0	1.0	1.0
15.....	7.944×10^{-3}	5.667×10^{-3}	1.041×10^{-2}
16.....	6.028×10^{-1}	1.000×10^{-1}	1.425×10^{-1}
17.....	8.901×10^{-3}	4.667×10^{-3}	4.047×10^{-3}
18.....	7.070×10^{-2}	3.283×10^{-2}	1.915×10^{-2}
19.....	3.718×10^{-3}	2.317×10^{-2}*	6.392×10^{-3}
20.....	6.451×10^{-2}	8.333×10^{-2}	5.887×10^{-2}
21.....	4.169×10^{-5}	1.367×10^{-2}*	1.730×10^{-4}
22.....	2.958×10^{-3}	5.817×10^{-2}*	3.166×10^{-3}
23.....	2.817×10^{-4}	2.433×10^{-2}*	0.0
24.....	1.318×10^{-2}	6.200×10^{-2}	2.481×10^{-2}
25.....	6.901×10^{-3}	1.800×10^{-2}	2.309×10^{-2}
26.....	8.901×10^{-1}	7.767×10^{-1}	9.661×10^{-1}
27.....	2.344×10^{-3}	4.500×10^{-3}	1.773×10^{-3}
28.....	5.014×10^{-2}	3.567×10^{-2}	5.591×10^{-2}

NOTE.—Abundances normalized to Si = 1.
[a] Asterisk denotes upper limit.

abundances. Spectra of boron, carbon, oxygen, and iron are shown in Figure 10 for two modulation levels, 450 and 800 MV. In case of carbon, the normalization coefficient in the LB component (eq. [1]) is fixed as $a(6, 12) = 6.35 \times 10^{-4}$ cm^{-2} s^{-1} sr^{-1} for $\eta = 1$. The calculated sub-Fe/Fe ratio is plotted in Figure 11. Since the elemental abundances are tuned at both high and low energies, it agrees well with data. In the intermediate region at $\sim$1 GeV nucleon^{-1}, the agreement could be improved by taking E_b smaller than the currently assumed 500 MeV (e.g., adopting $E_b = 400$ MeV may raise it by $\sim$10%, similar to the change in the B/C ratio; Fig. 3*b*).

The important result (Fig. 9) is that CR source and LB source abundances of all major elements ($_6$C, $_8$O, $_{10}$Ne, $_{12}$Mg, $_{14}$Si, $_{16}$S, $_{18}$Ar, $_{20}$Ca, $_{26}$Fe, and $_{28}$Ni) are in good agreement with each other. Abundances of the Si group, $_{20}$Ca, $_{26}$Fe, and $_{28}$Ni are near the solar system abundances. Abundances of other elements in Galactic CR and LB sources are mostly consistent with each other and with solar system abundances, within a factor of 2. Relative to silicon, $_6$C, $_7$N, $_8$O, $_{10}$Ne, and $_{16}$S are underabundant in both CR and LB sources. This corresponds to the well-known first ionization potential or volatility correlation (see, e.g., Meyer, Drury, & Ellison 1998). Nitrogen in CR and LB sources differs by a factor of $\sim$3, which may be connected with production cross section errors affecting propagation of the Galactic CR component (see discussion in the Appendix).

Secondary nuclei $_{19}$K, $_{21}$Sc, $_{22}$Ti, and $_{23}$V appear to be overabundant in the LB sources relative to the solar system (shown as upper limits in Fig. 9*a*), although the derived absolute LB abundances are not large. The derived LB abundance of $_{22}$Ti does not exceed that of $_{24}$Cr, while the derived abundances of $_{21}$Sc and $_{23}$V are not larger than that of $_{25}$Mn (Fig. 9*b*). One possible reason for this excess is the uncertainty in the production cross sections, which is especially large for these nuclei. Sometimes there is no measurement at all; in this case, one can use only phenomenological systematics, which are frequently wrong by a factor of 2 or even more, and/or predictions by Monte Carlo codes. Often, there is only one measurement at $\sim$600 MeV nucleon^{-1}, which has to be extrapolated in both directions.[5] This allows only a nearly flat Webber-type or Silberberg-Tsao–type extrapolation (see Silberberg, Tsao, & Barghouty 1998 and their code YIELDX_011000.FOR, Version 2000), while the real cross sections usually have large resonances below several hundred MeV and decrease with energy above a few GeV (see, e.g., Moskalenko et al. 2001a). We note that Davis et al. (2000) used semiempirical cross sections based on Webber, Kish, & Schrier (1990b) and also predicted fluxes of sub-Fe elements that are too low.

An estimate of the overall error, which is reflected in the derived LB source abundances, can be obtained by assuming the complete absence of $_{19}$K, $_{21}$Sc, $_{22}$Ti, and $_{23}$V in the LB source (shown by crosses in Fig. 9). In this case, the discrepancy between the calculated propagated CR

[5] Only the following reactions are well measured (see compilation by Mashnik et al. 1998), on a sample of natural iron consisting mostly of ^{56}Fe: $p + {}^{\rm nat}\mathrm{Fe} \rightarrow {}^{46}_{21}\mathrm{Sc}, {}^{47}_{21}\mathrm{Sc}, {}^{48}_{23}\mathrm{V}, {}^{48}_{24}\mathrm{Cr}, {}^{51}_{24}\mathrm{Cr}$; we use our fits to these data. Reactions producing other isotopes of $_{21}$Sc, $_{22}$Ti, and $_{23}$V by $^{56}_{26}$Fe, $^{55}_{25}$Mn, and $^{52}_{24}$Cr have only one or two measurements. There are no data available on the production of $_{21}$Sc, $_{22}$Ti, and $_{23}$V by $^{54}_{26}$Fe, $^{53}_{25}$Mn, and $_{24}$Cr isotopes (except $^{52}_{24}$Cr), on production of $_{21}$Sc and $_{22}$Ti by $^{49}_{23}$V, and on production of $_{21}$Sc by $_{22}$Ti. These poorly known cross sections contribute to errors on the production of sub-Fe elements at low energies.

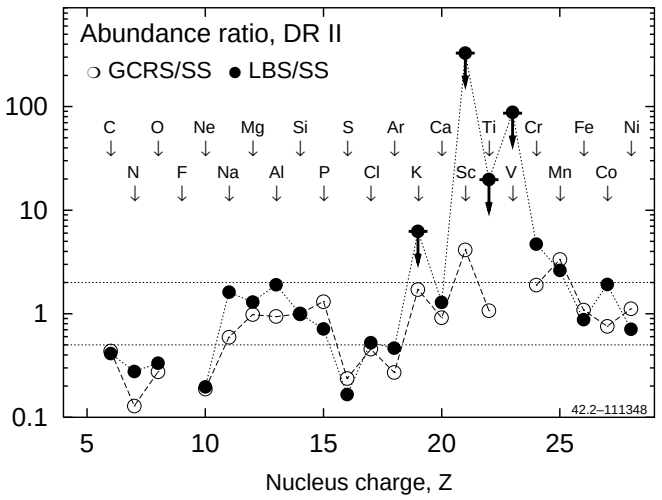

FIG. 9*a*

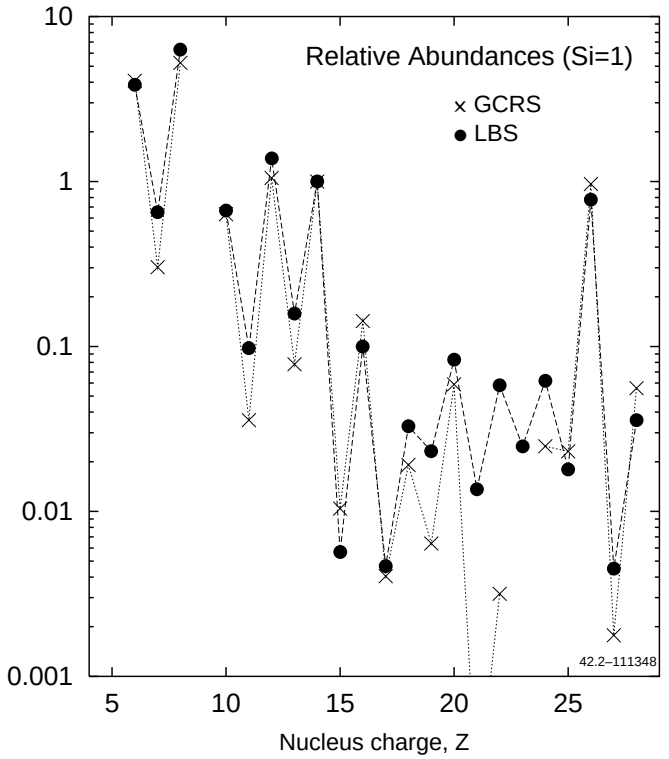

FIG. 9*b*

FIG. 9.—(*a*) Derived abundance ratios (DR II model) Galactic CR source/solar system (GCRS/SS) and LB-source/solar system (LBS/SS), normalized to silicon. Relative abundances for K, Sc, Ti, and V are shown as upper limits. Solar system abundances from Grevesse & Sauval (1998). Horizontal lines are plotted at $\frac{1}{2}$ and 2. (*b*) Derived GCRS and LBS abundances normalized to silicon.

abundances of $_{19}$K, $_{21}$Sc, $_{22}$Ti, and $_{23}$V and those measured is below 20%, and it can be *removed* by allowing the production cross sections to increase at low energies by ~15%–20%, which seems plausible.

Another possibility is errors in flux measurements of the rare CR species. Figure 12 shows the calculated abundances[6] tuned at low energies to the *ACE* and *Ulysses* data. *Ulysses* and *ACE* measurements are not always in agreement. Note that even for such an abundant nucleus as iron, which is the main contributor to the sub-Fe group, the discrepancy exceeds 10%, while the disagreement in abundance of $_{21}$Sc is ~30%.

The derived source overabundance of sub-Fe elements in the LB could also, in principle, arise from composition differences between the ISM in the LB and the solar or Galactic average ISM. This is suggested by the fact that the relative abundances of secondary elements in the LB sources are systematically larger than those in the Galactic CR sources (Fig. 9). However, the factors required in case of, e.g., $_{22}$Ti (Ti/Fe ~5%, compared to solar or SN 0.1%) appear much larger than could reasonably be expected even for unusual SN types. A similar effect may be caused by a specific correlation between source and gas density distributions (Ptuskin & Soutoul 1990).

6.2. *Isotopic Distributions in CRs*

Be and B isotopes are all assumed to be secondary; thus, there is no possibility to tune them. The DR II model calculation shows perfect agreement with the data on relative isotopic abundances of Be and B (Fig. 13). This is in contrast with a standard reacceleration model, in which we obtained a 15% discrepancy with relative abundances of ^{7}Be and ^{9}Be isotopes (Strong & Moskalenko 2001).

Abundances of stable isotopes of other elements are not very conclusive because they are present in the sources, but O and Si isotopic distributions still agree very well with data (Webber et al. 1996; Webber, Lukasiak, & McDonald 1997; DuVernois et al. 1996; Hesse et al. 1996; Wiedenbeck et al. 2001), assuming that only ^{16}O and ^{28}Si isotopes are present in the LB component. C and N isotopic distributions do not agree too well (Fig. 13), but this may point to a problem with cross sections. The calculated ratio $^{13}\mathrm{C}/^{12}\mathrm{C} \sim 0.11$ at 120 MeV nucleon^{-1} ($\Phi = 500$ MV) in the model with LB contribution is still a factor ~1.5 too large compared to the measured values, 0.0629 ± 0.0033 (*Voyager* data at 50–130 MeV nucleon^{-1}; Webber et al. 1996) and 0.078 ± 0.011 (*Ulysses* data at 100–200 MeV nucleon^{-1}; DuVernois et al. 1996), which may be connected in part with overproduction of ^{13}C by ^{15}N. (A discussion of the cross section uncertainties for C and N isotopes is given in the Appendix.) If we replace the cumulative cross section $^{15}\mathrm{N} + p \rightarrow {}^{13}\mathrm{C}$ with cross section $^{14}\mathrm{N} + p \rightarrow {}^{13}\mathrm{C}$, the calculated ratio $^{13}\mathrm{C}/^{12}\mathrm{C}$ will be lowered by 10%, as estimated (see the Appendix and Fig. 15). Assuming the absence of the isotope ^{13}C in the Galactic CR sources gives another 10% reduction. Altogether, these corrections yield $^{13}\mathrm{C}/^{12}\mathrm{C} \sim 0.09$, close to the data.

Figure 14 shows calculated $^{10}\mathrm{Be}/^{9}\mathrm{Be}$, $^{26}\mathrm{Al}/^{27}\mathrm{Al}$, $^{36}\mathrm{Cl}/\mathrm{Cl}$, and $^{54}\mathrm{Mn}/\mathrm{Mn}$ ratios, usually used as "radioactive clocks" in CRs, for a halo size $z_h = 4$ kpc versus data. In case of Be, Al, and Cl, the agreement with the most accurate low-energy

[6] Calculated Li abundance in the plot shows only secondary lithium produced in CRs.

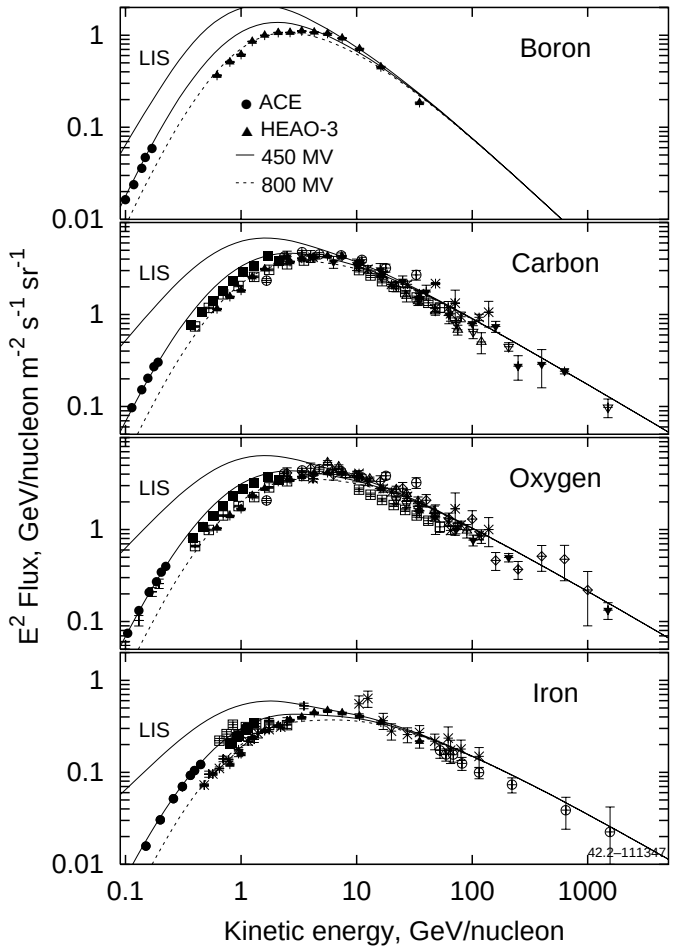

FIG. 10.—Spectra of boron, carbon, oxygen, and iron (*from top to bottom*) calculated with LB contribution (DR II model). *Upper curves*: LIS; *lower curves*: modulated using force field approximation with $\Phi = 450$ MV (*solid curves*) and $\Phi = 800$ MV (*dashed curves*). Data: *ACE* (Davis et al. 2000, 2001) and *HEAO 3* (Engelmann et al. 1990). For other references, see Stephens & Streitmatter (1998) (symbols are changed).

data by *ACE* is very good and all the ratios are consistent with each other, indicating that $z_h = 4$ kpc is a good estimate. Higher energy data by ISOMAX (Be) are also consistent with calculations, considering the large error bars.

The ^{54}Mn/Mn ratio indicates a somewhat smaller halo, but this may be related to uncertainty in its half-life and/or production cross section. The half-life of ^{54}Mn against β^--decay is the most uncertain among the four radioactive isotopes—it is the only one that is not measured directly. It is derived indirectly based on β^+-decay branch half-life, which yields an estimate $t_{1/2}(\beta^-) = [6.3 \pm 1.3(\text{stat}) \pm 1.1(\text{theor})] \times 10^5$ yr (Wuosmaa et al. 1998). In case only the half-life is wrong, to get the ^{54}Mn/Mn ratio consistent with lighter element ratios and with *ACE* data (for $z_h = 4$ kpc) requires $t_{1/2}(\beta^-) \sim 2$ Myr (Fig. 14). Another estimate of the ^{54}Mn partial half-life based on CR propagation calculations gives ~1–2 Myr (DuVernois 1997). Apart from the half-life, a possible source of errors can be production cross sections of Mn isotopes. The fact that the propagated isotopic abundance of ^{53}Mn, ^{53}Mn/Mn = 0.50, is correct (^{53}Mn is a K-capture isotope that is absent in the ISM) indicates that some important production channels of ^{54}Mn and ^{55}Mn may be not calculated correctly. (For instance, in the case of stable ^{55}Mn, we have a freedom to choose its abundance in

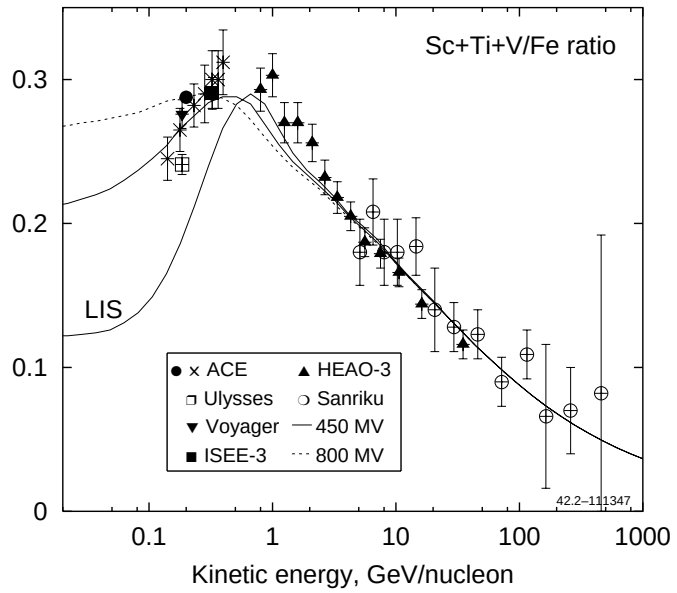

FIG. 11.—Sub-Fe/Fe ratio calculated with LB contribution (DR II model) and $E_b = 500$ MeV nucleon^{-1}. *Lower curve*: LIS; *upper curves*: modulated using force field approximation with $\Phi = 450$ MV (*solid curve*) and $\Phi = 800$ MV (*dashed curve*). Data: *ACE* (Wiedenbeck et al. 2001; Davis et al. 2000), *Ulysses* (DuVernois & Thayer 1996), *Voyager* (Lukasiak, McDonald, & Webber 1997), *ISEE 3* (Leske 1993), *HEAO 3* (Engelmann et al. 1990), and Sanriku (Hareyama et al. 1999).

the LB component at low energies, which may compensate for underproduction of this isotope in CRs. Meanwhile, this LB ^{55}Mn does not produce any ^{54}Mn.) Only the reaction $^{\text{nat}}\text{Fe} + p \rightarrow {}^{54}\text{Mn}$ on a natural sample of Fe has been

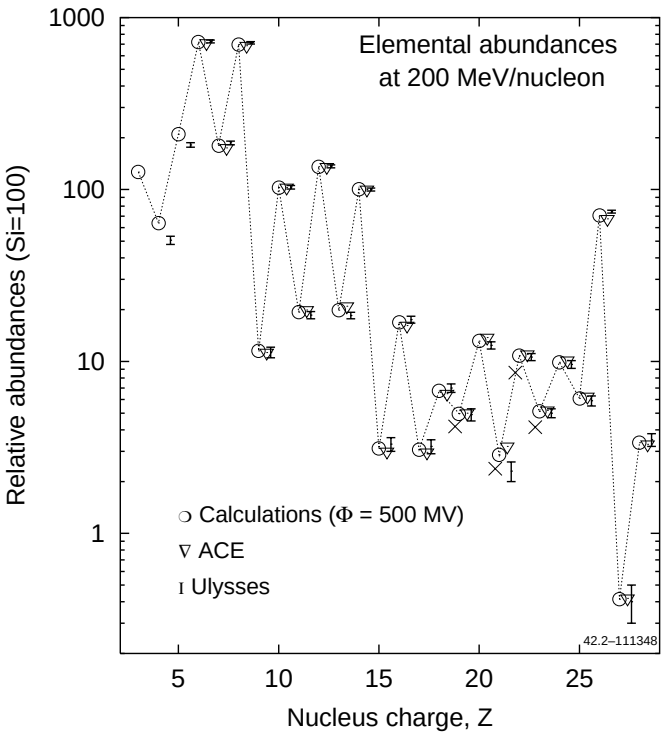

FIG. 12.—Propagated elemental abundances at 200 MeV nucleon^{-1} with LB contribution (DR II model). Crosses show the calculated abundances assuming no K, Sc, Ti, and V in the LB source. Data: *ACE* (Wiedenbeck et al. 2001) and *Ulysses* (DuVernois & Thayer 1996).

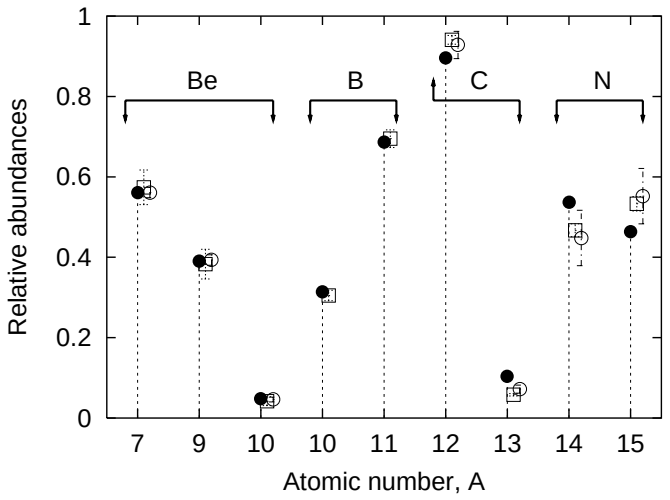

FIG. 13.—Be, B, C, and N isotope distribution as calculated in DR II model (*filled circles*) at ~70–150 MeV nucleon^{-1} and a modulation potential $\Phi = 450$–500 MV compared to the data. Be data: *Ulysses* (Connell 1998) and *Voyager* (Lukasiak et al. 1999). B data: *Voyager* (Lukasiak et al. 1999). C and N data: *Voyager* (Webber et al. 1996) and *Ulysses* (DuVernois et al. 1996).

measured well enough (see compilation by Mashnik et al. 1998). The cross section $^{55}\mathrm{Mn} + p \rightarrow {}^{54}\mathrm{Mn}$ has only one point measured by Webber et al. (1998b); besides, it seems too low compared to similar neutron knockout reactions on isotopes of Fe and Cr. Reactions $^{55}\mathrm{Fe} + p \rightarrow {}^{54}\mathrm{Mn}$ and $^{57}\mathrm{Fe} + p \rightarrow {}^{54}\mathrm{Mn}$ are not measured at all. Similarly, only one ^{55}Mn major production cross section, $^{56}\mathrm{Fe} + p \rightarrow {}^{55}\mathrm{Mn}$ has even one point measured.

7. DISCUSSION

The proton spectrum at low energies still remains uncertain. The only secondaries produced below the antiproton production threshold are positrons and γ-rays. However, the positron spectrum *alone* cannot provide conclusive information on the proton spectrum on a large scale, because (1) the large energy losses of positrons mean that the positron spectrum by its nature is local and (2) there are possibly sources of primary positrons, such as pulsars. Diffuse γ-rays can provide a tool to test the spectrum of protons in distant regions, but the a priori unknown contribution of electrons via inverse Compton scattering and bremsstrahlung complicates the picture. A test of the He spectrum at energies below ~10 GeV nucleon^{-1} can be made using the CR deuteron and ^{3}He measurements similarly to what was done in this paper for heavier nuclei. We plan to address this issue in future work.

We should mention that there is another possibility to get the correct antiproton flux in reacceleration models, which is to introduce an additional proton component at energies up to approximately 20 GeV. The latter energy is above the antiproton production threshold and effectively produces antiprotons at ~2 GeV and below. The intensity and spectral shape of this component could be derived by combining restrictions from antiprotons and diffuse γ-rays. Interestingly, this kind of spectrum was used in our HEMN model (hard electrons and modified nucleons; Strong, Moskalenko, & Reimer 2000) to match the spectrum of diffuse γ-rays as observed by EGRET (Hunter et al. 1997). The advantage of this approach is that the diffuse γ-rays that we observe carry information on the large-scale Galactic spectrum of CRs (producing antiprotons), while particles that we measure may reflect only the local region.

One more (nonstandard) interpretation is that the solar modulation is weaker than assumed and that this would eliminate the need for a LB component. (A cornerstone of the current theories of heliospheric modulation is the local interstellar spectrum, which is not known but taken a priori.) With a modulation potential as small as ~200 MV, one can obtain a consistent reacceleration model combining B/C, antiprotons, and other species simultaneously. To get an agreement with nucleon spectral data, the injection spectra in such a model should be flatter at low energies than the usually adopted power law in rigidity.

Recently there has appeared some indication that the atmospheric contribution to the antiproton flux measured in the upper atmosphere is underestimated. Monte Carlo simulations of the hadron cascade development in the upper atmosphere have shown that the antiproton flux induced by *p-A* reactions on air nuclei is larger, *at least*, by ~30% (Huang, Derome, & Buénerd 2001) compared to often employed calculations with analytical production cross sections. This means that the flux of antiprotons in CRs in reality may be *lower* at the top of the atmosphere by at least 25%–30%. If the latter is true, the reacceleration model (even without an LB component) could still be the best one to describe propagation of nucleon species in the Galaxy. The inclusion of all known effects, such as subthreshold antiproton production on the abundant atmospheric N and O, may be important for evaluation of the correct atmospheric background.

We note that Donato et al. (2001) claim to have obtained agreement with antiproton measurements in a reacceleration plus convection model using the parameters derived from B/C and sub-Fe/Fe ratios (Maurin et al. 2001). Apart from having one more free parameter (convection *plus* reacceleration), they in fact fitted B/C and sub-Fe/Fe ratios only at high energies (since in their fitting procedure the high-energy data outweigh the few low-energy points). Their calculated ratios at low energies are higher than the *Voyager* and *ACE* data by approximately 20%, or about 6 σ (see Figs. 3 and 4 in Maurin et al. 2001). This is, however, where most of the problem lies. Besides, in their nuclear reaction treatment, they use the semiempirical cross sections by Webber et al. (1990b), which are not particularly accurate at low energies, while reacceleration models are sensitive to low-energy behavior of the cross sections.

8. CONCLUSION

In a previous paper, we have shown that new, more accurate measurements of the CR antiproton flux pose a challenge to existing CR propagation models. In particular, the antiproton flux and B/C ratio appear to be inconsistent with measurements when computed in standard diffusion/reacceleration models. In this paper, we have demonstrated that this discrepancy can be resolved if some part of the CRs that we measure near the Earth consists of a fresh component accelerated in the LB. The independent evidence for SN activity in the solar vicinity in the last few Myr supports this idea.

Combining the measurements of the antiproton flux *and* B/C ratio to fix the diffusion coefficient, we have been able

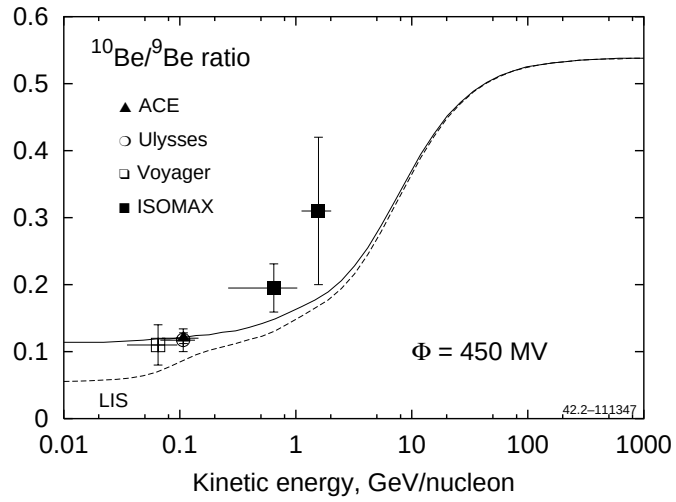

FIG. 14*a*

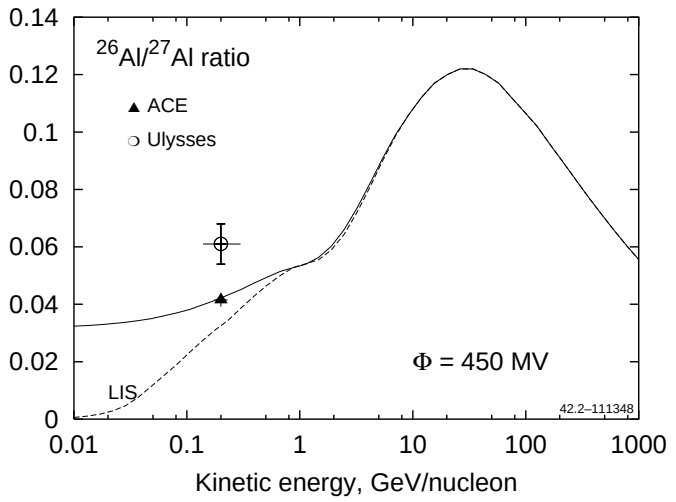

FIG. 14*b*

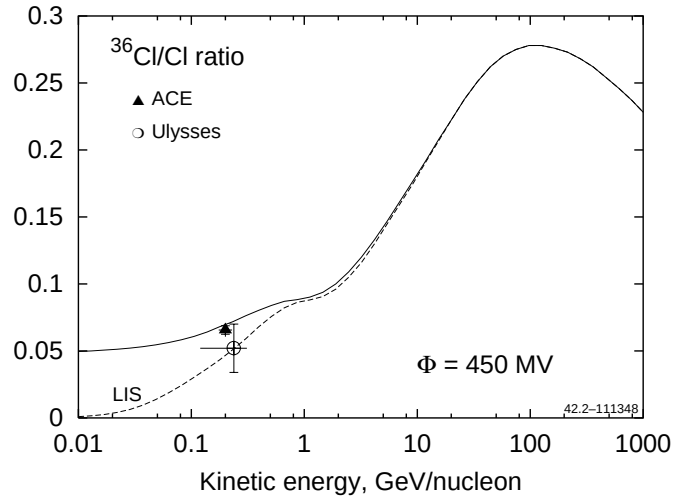

FIG. 14*c*

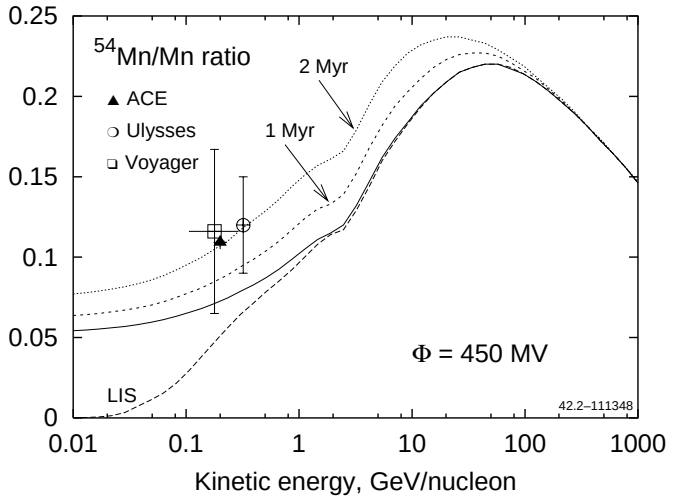

FIG. 14*d*

FIG. 14.—"Radioactive clocks," isotopic ratios in CRs, as calculated in DR II model for $z_h = 4$ kpc. *Dashed curves*: LIS; *solid curves*: modulated ($\Phi = 450$ MV). Mn plot (*d*) also shows the ratio calculated for two half-lives, $t_{1/2} = 1$ and 2 Myr, that are different from the adopted $t_{1/2} = 0.63$ Myr. Be data: *Ulysses* (Connell 1998), *Voyager* (Lukasiak et al. 1999), *ACE* (Binns et al. 1999), and ISOMAX (Hams et al. 2001; de Nolfo et al. 2001). Al data: *Ulysses* (Simpson & Connell 1998) and *ACE* (Wiedenbeck et al. 2001). Cl data: *Ulysses* (Connell, DuVernois, & Simpson 1998) and *ACE* (Wiedenbeck et al. 2001). Mn data: *Ulysses* (DuVernois 1997), *Voyager* (Lukasiak et al. 1997), and *ACE* (Wiedenbeck et al. 2001).

to construct a model consistent with measurements of important nuclei ratios in CRs and to derive elemental abundances in the LB. Calculated isotopic abundance distributions of Be and B are in perfect agreement with CR data. The abundances of three radioactive isotopes in CRs that are often used as radioactive clocks to determine the Galactic halo size, ^{10}Be, ^{26}Al, and ^{36}Cl, are all consistent and indicate a halo size $z_h \sim 4$ kpc, based on the most accurate data by *ACE* spacecraft. ^{54}Mn indicated a smaller halo, but this may be related to its half-life uncertainty and/or cross section errors. The derived fraction of the LB component in CRs is small, compared to that in Galactic CRs, and has a steep spectrum with a cutoff above several hundred MeV/nucleon. Other experimental data (except maybe the overabundance of Sc, Ti, and V) do not contradict this hypothesis. The derived source overabundance of sub-Fe elements in the LB may be caused by trivial uncertainties in the production cross sections or could, in principle, arise from composition and/or evolution differences between the ISM in the LB and the solar or Galactic average ISM. (The LB may have evolved during the Sun's lifetime of 4.5 Gyr.) This is suggested by the fact that the derived relative abundances of secondary elements in the LB sources are systematically larger than those in the Galactic CR sources (see, e.g., Savage et al. 2002 on derivation of the interstellar ^{12}C/^{13}C ratio).

The production cross sections, if measured accurately, would help to distinguish between the different hypotheses; as of now, many important channels are not known accurately enough. Such cross section errors lead to errors in important isotopic ratios, which, in turn, are translated into errors in propagation parameters. In our treatment of Be and B production cross sections, as well as of some isotopes of other elements, we use all available data and our own fits to them, which should be more accurate than semiempirical systematics by Webber et al. and Silberberg et al.

The authors are grateful to M. Wiedenbeck for providing the *ACE* isotopic abundances. I. V. M. is grateful to the Gamma-Ray Group of the Max-Planck-Institut für extraterrestrische Physik, where a part of this work has been done, for hospitality. I. V. M. and S. G. M. acknowledge partial support from a NASA Astrophysics Theory Program grant.

APPENDIX

PRODUCTION CROSS SECTIONS OF ISOTOPES OF CARBON AND NITROGEN

The production cross section of the most abundant ^{12}C isotope is one of the most poorly known. All the data available to us on its production by ^{16}O and nitrogen isotopes on protons are summarized in Table 3. The data include also production of ^{12}B and ^{12}N, which decay to ^{12}C with branching ratio 0.98, and ^{13}O, which decays with branching ratio 0.12.

Data on the production of ^{13}C are somewhat more extensive, but some important channels are not measured accurately enough. Most of the data available are summarized in Table 4. The data also include production of ^{13}N, which decays to ^{12}C with branching ratio 1. The production cross section of ^{13}B is very small, fractions of a millibarn. Fortunately, there are data on production of ^{13}N by protons on natural samples of oxygen and nitrogen (see compilation by Mashnik et al. 1998), which contain mostly ^{16}O and ^{14}N isotopes, respectively. The ^{13}N production cross section data probably also include production of ^{13}O, but the latter cross section must be very small (0.17 mbarn at 2100 MeV nucleon^{-1}).

The production cross section of the most abundant ^{14}N isotope is also poorly known. All the data available to us are summarized in Table 5. The compiled data also include production of ^{14}C and ^{14}O, which decay to ^{14}N with branching ratio 1.

The main contributor to the production cross section of ^{15}N is ^{16}O (Table 6). The direct and indirect (via ^{15}O) production cross sections are almost equal. The channel $p + {}^{16}\mathrm{O} \rightarrow {}^{15}\mathrm{O}$ is well studied, since there is a large amount of data obtained on a natural sample of oxygen (see compilation by Mashnik et al. 1998).

The cumulative (sum over all channels) production cross sections of carbon and nitrogen isotopes, multiplied by the flux of the corresponding primary isotope in CRs at 1 GeV nucleon^{-1}, are shown in Figure 15. The main contributor to the production of secondary carbon and nitrogen is ^{16}O, accounting for about 80% in the case of nitrogen isotopes. However, in the case of carbon, disintegration of ^{16}O gives only about 50%, with an essential contribution from nitrogen isotopes (and ^{13}C, in the case of ^{12}C).

The contribution of ^{15}N to the production of ^{13}C is especially large (Table 4). This is based on only one experimental point, which seems too large compared to the production cross sections on ^{14}N and ^{16}O. This indicates that the reason for the large fraction of ^{13}C in calculated CR abundances compared to the measurements (see §§ 2 and 6) may be errors in the cross sections.

There are more examples of discrepancies in ^{13}C and ^{14}N production cross sections (marked by asterisks in Tables 4 and 5). The production cross section of ^{13}C by ^{22}Ne at 580 MeV nucleon^{-1} differs significantly from that at 400 MeV nucleon^{-1}. The cross section of ^{13}C by ^{26}Mg measured by the same group at 370 and 576 MeV nucleon^{-1} differs by a factor of 4 (6.3 vs. 25 mbarn). A similar situation occurs with ^{14}C production by ^{22}Ne at 400, 580, and 894 MeV nucleon^{-1} and by ^{26}Mg at 371 and 576 MeV nucleon^{-1} (3.5 vs. 9 mbarn). Fortunately, these latter cross sections do not contribute much to production of ^{13}C and ^{14}N in CRs, but these discrepancies indicate the degree of overall uncertainty in the production cross sections.

Cross section errors in production of carbon may lead to errors in the B/C ratio, which, in turn, are translated into errors on the propagation parameters. Because the CR measurements are now rather accurate, the errors in the cross sections may cause many standard deviations when comparing the model calculations with CR data.

It is clear that a more systematic approach to calculated cross sections is required, e.g., using evaluated cross sections in future similar work instead of only scarce experimental data, calculations by stand-alone nuclear reaction models, or

TABLE 3
COLLECTION OF ^{12}C PRODUCTION CROSS SECTION DATA ON PROTONS

Primary Nucleus	Secondary Nucleus	Energy (MeV nucleon^{-1})	Cross Section (mbarn)	Error (mbarn)	Reference
^{14}N	^{12}C	377	56.90	0.05[a]	1
		516	52.10	0.05[b]	2
^{15}N	^{12}C	373	30.00	0.05[a]	1
^{16}O	^{12}C	389	33.90	0.05[a]	1
		516	33.60	0.05[b]	2
		2100	32.30	4.80	3
	^{12}B	516	1.10	0.30[b]	2
		2100	1.45	0.17	3
^{14}N	^{12}N	516	1.10	0.30[b]	2
^{16}O	^{12}N	516	0.30	0.30[b]	2
		2100	0.40	0.07	3

[a] Relative error.
[b] Relative error as indicated in Webber et al. 1998a.
REFERENCES.—(1) Webber et al. 1998a; (2) Webber, Kish, & Schrier 1990a; (3) Olson et al. 1983.

TABLE 4

COLLECTION OF ^{13}C PRODUCTION CROSS SECTION DATA ON PROTONS

Primary Nucleus	Secondary Nucleus	Energy (MeV nucleon^{-1})	Cross Section (mbarn)	Error (mbarn)	Reference
^{14}N	^{13}C	377	7.60	0.05[a]	1
		516	9.60	0.05[b]	2
^{15}N	^{13}C	373	35.30*	0.05[a]	1
^{16}O	^{13}C	389	17.40	0.05[a]	1
		516	18.00	0.05[b]	2
		2100	17.80	1.70	3
^{20}Ne	^{13}C	414	15.30	0.05[a]	1
		534	15.70	0.05[b]	2
^{22}Ne	^{13}C	377	17.80	1.40	4
		401	15.30*	0.05[a]	1
		581	21.90*	1.90	4
		894	19.00	1.60	4
^{26}Mg	^{13}C	371	6.30*	1.20	4
		576	25.00*	2.80	4
^{nat}N (^{14}N)	^{13}N		Multiple values		5
^{14}N	^{13}N	377	7.40	0.10[a]	1
		516	7.50	0.10[b]	2
^{15}N	^{13}N	373	4.30	0.30[a]	1
^{nat}O (^{16}O)	^{13}N		Multiple values		5
^{16}O	^{13}N	389	4.60	0.20[a]	1
		516	5.70	0.20[b]	2
		2100	4.49	0.46	3
^{20}Ne	^{13}N	414	5.10	0.20[a]	1
		534	4.10	0.20[b]	2
^{22}Ne	^{13}N	377	0.50	0.10	4
		401	1.60	0.20[a]	1
		581	0.50	0.10	4
		894	0.70	0.20	4
^{24}Mg	^{13}N	610	6.00	0.20[b]	2
^{26}Mg	^{13}N	371	0.30	0.10	4
		576	0.10	0.10	4

NOTE.—Asterisk indicates discrepancy in the data.

[a] Relative error.

[b] Relative error as indicated in Webber et al. 1998a.

REFERENCES.—(1) Webber et al. 1998a; (2) Webber et al. 1990a; (3) Olson et al. 1983; (4) Chen et al. 1997; (5) Compilation by Mashnik et al. 1998.

TABLE 5

COLLECTION OF ^{14}N PRODUCTION CROSS SECTION DATA ON PROTONS

Primary Nucleus	Secondary Nucleus	Energy (MeV nucleon^{-1})	Cross Section (mbarn)	Error (mbarn)	Reference
^{15}N	^{14}N	373	27.60	0.05[a]	1
^{16}O	^{14}N	389	31.10	0.05[a]	1
		516	31.00	0.05[b]	2
		2100	31.00	3.30	3
^{20}Ne	^{14}N	414	25.80	0.05[a]	1
^{22}Ne	^{14}N	401	11.60	0.10[a]	1
^{15}N	^{14}C	373	10.30	0.05[a]	1
^{16}O	^{14}C	389	1.70	0.10[a]	1
		516	1.70	0.10[b]	2
		2100	3.69	0.38	3
^{20}Ne	^{14}C	414	2.20	0.10[a]	1
		534	2.30	0.10[b]	2
^{22}Ne	^{14}C	377	8.10	0.70	4
		401	7.70	0.05[a]	1
		581	10.20	1.20	4
		894	8.60	0.90	4

TABLE 5—*Continued*

Primary Nucleus	Secondary Nucleus	Energy (MeV nucleon^{-1})	Cross Section (mbarn)	Error (mbarn)	Reference
^{26}Mg	^{14}C	371	3.50*	0.70	4
		576	9.00*	1.30	4
^{16}O	^{14}O	389	1.30	0.30[a]	1
		516	1.20	0.30[b]	2
		2100	0.75	0.12	3
^{20}Ne	^{14}O	534	1.00	0.30[b]	2
^{24}Mg	^{14}O	610	1.50	0.30[b]	2

NOTE.—Asterisks indicates discrepance in the data.
[a] Relative error.
[b] Relative error as indicated in Webber et al. 1998a.
REFERENCES.—(1) Webber et al. 1998a; (2) Webber et al. 1990a; (3) Olson et al. 1983; (4) Chen et al. 1997.

TABLE 6
COLLECTION OF ^{15}N PRODUCTION CROSS SECTION DATA ON PROTONS

Primary Nucleus	Secondary Nucleus	Energy (MeV nucleon^{-1})	Cross Section (mbarn)	Error (mbarn)	Reference
^{16}O	^{15}N	389	33.60	0.05[a]	1
		516	34.90	0.05[b]	2
		2100	34.30	3.30	3
^{20}Ne	^{15}N	414	24.00	0.05[a]	1
		534	27.80	0.05[b]	2
^{22}Ne	^{15}N	377	36.20	2.10	4
		401	32.90	0.05[a]	1
		581	39.00	2.50	4
		894	33.50	2.10	4
^{24}Mg	^{15}N	610	14.00	0.10[b]	2
^{26}Mg	^{15}N	371	19.70*	2.10	4
		576	29.90*	3.00	4
^{22}Ne	^{15}C	377	0.70	0.20	4
		581	0.80	0.20	4
		894	0.60	0.10	4
^{26}Mg	^{15}C	371	0.90	0.30	4
		576	0.40	0.30	4
^{nat}O (^{16}O)	^{15}O		Multiple values		5
^{16}O	^{15}O	389	30.70	0.05[a]	1
		516	30.30	0.05[b]	2
		2100	27.30	2.60	3
^{20}Ne	^{15}O	414	14.90	0.10[a]	1
		534	16.20	0.10[b]	2
^{21}Ne	^{15}O	520	7.80	0.30[a]	6
^{22}Ne	^{15}O	377	2.00	0.30	4
		401	1.60	0.20[a]	1
		581	1.60	0.30	4
		894	2.80	0.40	4
^{22}Na	^{15}O	520	10.90	0.30[a]	6
^{23}Na	^{15}O	517	11.10	0.30[a]	6
^{24}Mg	^{15}O	610	8.60	0.10[b]	2
^{25}Mg	^{15}O	514	6.00	0.30[a]	6
^{26}Mg	^{15}O	371	1.10	0.30	4
		576	0.20	0.20	4
^{26}Al	^{15}O	508	4.10	0.30[a]	6
^{27}Al	^{15}O	511	7.10	0.20[a]	6
^{28}Si	^{15}O	506	5.60	0.12[a]	6
^{29}Si	^{15}O	508	2.40	0.30[a]	6

NOTE.—Asterisk indicates discrepancy in the data.
[a] Relative error.
[b] Relative error as indicated in Webber et al. 1998a.
REFERENCES.—(1) Webber et al. 1998a; (2) Webber et al. 1990a; (3) Olson et al. 1983; (4) Chen et al. 1997; (5) Compilation by Mashnik et al. 1998; (6) Webber et al 1998b.

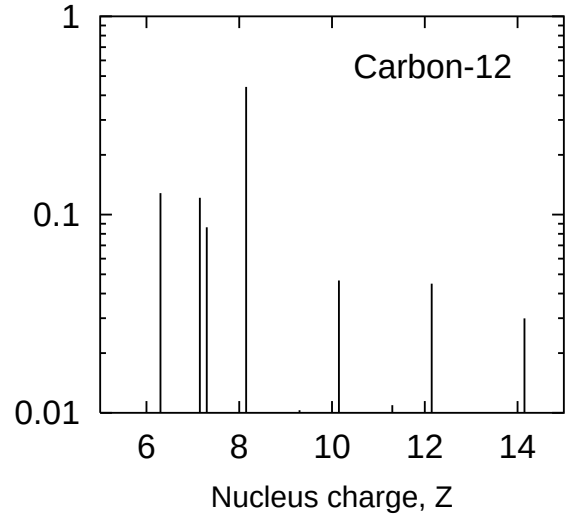

FIG. 15*a*

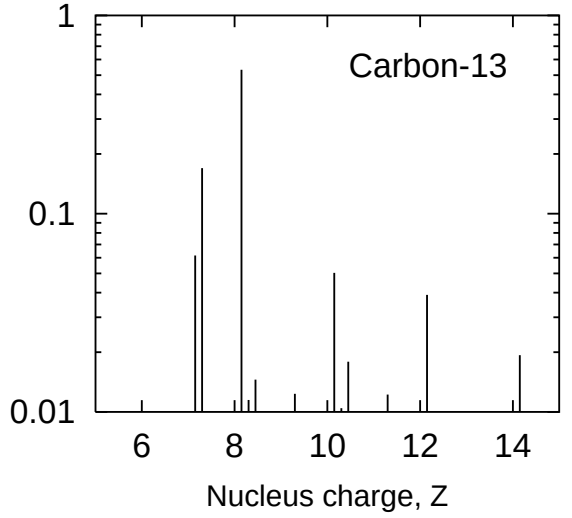

FIG. 15*b*

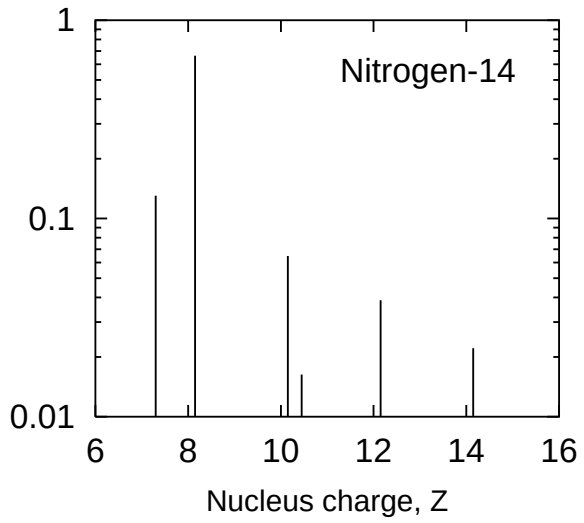

FIG. 15*c*

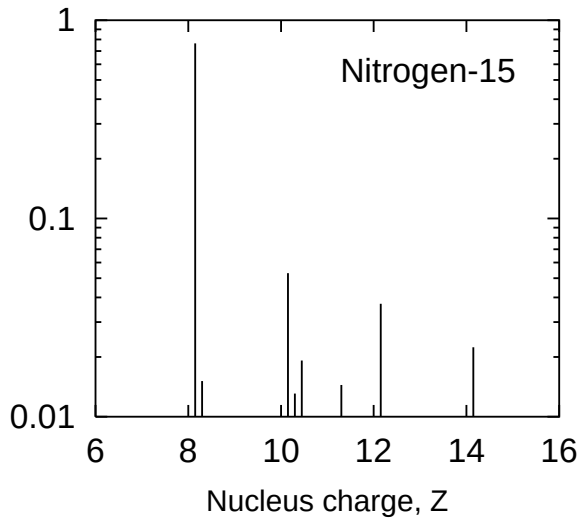

FIG. 15*d*

FIG. 15.—Relative contributions of heavier isotopes to production of C and N isotopes are shown. These contributions are determined from cumulative cross sections of C and N isotopes weighted with the flux of corresponding primary isotope in CRs at 1 GeV nucleon^{-1}. The contributions of isotopes of a given element are indicated by separate lines. The scale gives the fraction of the C and N isotopes produced by a given primary isotope.

phenomenological systematics. Such evaluated data files (Mashnik et al. 1998) have proved to be useful, e.g., to study the production of radioisotopes for medical and industrial applications using high-power accelerators (Van Riper, Mashnik, & Wilson 2001). At present, neither available experimental data nor any of the current models or phenomenological systematics can be used alone to produce a reliable evaluated activation cross section library covering a wide range of target nuclides and incident energies. Instead, such an evaluated library may be created by constructing excitation functions using all available experimental data, along with calculations employing some of the most reliable codes in the regions of targets and incident energies where they are most applicable. When there are reliable experimental data, they, rather than model results, should be taken as the highest priority for the evaluation. The development of such evaluated data libraries for astrophysical applications is planned in the near future.

REFERENCES

Alcaraz, J., et al. 2000, Phys. Lett. B, 490, 27
Anders, E., & Grevesse, N. 1989, Geochim. Cosmochim. Acta, 53, 197
Asaoka, Y., et al. 2002, Phys. Rev. Lett., 88, 051101
Basini, G., et al. 1999, Proc. 26th Int. Cosmic-Ray Conf. (Salt Lake City), 3, 77
Benítez, N., Maíz-Apellániz, J., & Canelles, M. 2002, Phys. Rev. Lett., 88, 081101
Berghöfer, T. W., & Breitschwerdt, D. 2002, A&A, 390, 299
Binns, W. R., et al. 1999, Proc. 26th Int. Cosmic-Ray Conf. (Salt Lake City), 3, 21
Boezio, M., et al. 1999, ApJ, 518, 457
———. 2001, ApJ, 561, 787
Bogomolov, E. A., Lubyanaya, N. D., Romanov, V. A., Stepanov, S. V., & Shulakova, M. S. 1979, Proc. 16th Int. Cosmic-Ray Conf. (Kyoto), 1, 330
Bykov, A. M. 2001, Space Sci. Rev., 99, 317
Bykov, A. M., & Fleishman, G. D. 1992, MNRAS, 255, 269
Chen, C.-X., et al. 1997, ApJ, 479, 504
Connell, J. J. 1998, ApJ, 501, L59
Connell, J. J., DuVernois, M. A., & Simpson, J. A. 1998, ApJ, 509, L97

Davis, A. J., et al. 2000 in AIP Conf. Proc. 528, Acceleration and Transport of Energetic Particles Observed in the Heliosphere, ed. R. A. Mewaldt, J. R. Jokipii, M. A. Lee, E. Möbius, & T. H. Zurbuchen (New York: AIP), 421
———. 2001, Proc. 27th Int. Cosmic-Ray Conf. (Hamburg), 3971
de Nolfo, G. A., et al. 2001, Proc. 27th Int. Cosmic-Ray Conf. (Hamburg), 1659
Donato, F., Maurin, D., Salati, P., Barrau, A., Boudoul, G., & Taillet, R. 2001, ApJ, 563, 172
DuVernois, M. A. 1997, ApJ, 481, 241
DuVernois, M. A., Garcia-Munoz, M., Pyle, K. R., Simpson, J. A., & Thayer, M. R. 1996, ApJ, 466, 457
DuVernois, M. A., Simpson, J. A., & Thayer, M. R. 1996, A&A, 316, 555
DuVernois, M. A., & Thayer, M. R. 1996, ApJ, 465, 982
Engelmann, J. J., et al. 1990, A&A, 233, 96
Gleeson, L. J., & Axford, W. I. 1968, ApJ, 154, 1011
Golden, R. L., Horan, S., Mauger, B. G., Badhwar, G. D., Lacy, J. L., Stephens, S. A., Daniel, R. R., & Zipse, J. E. 1979, Phys. Rev. Lett., 43, 1196
Grevesse, N., & Sauval, A. J. 1998, Space Sci. Rev., 85, 161
Hams, T., et al. 2001, Proc. 27th Int. Cosmic-Ray Conf. (Hamburg), 1655
Hareyama, M., et al. 1999, Proc. 26th Int. Cosmic-Ray Conf. (Salt Lake City), 3, 105
Hesse, A., et al. 1996, A&A, 314, 785
Higdon, J. C., Lingenfelter, R. E., & Ramaty, R. 1998, ApJ, 509, L33
Huang, C. Y., Derome, L., & Buénerd, M. 2001, Proc. 27th Int. Cosmic-Ray Conf. (Hamburg), 1707
Hunter, S. D., et al. 1997, ApJ, 481, 205
Jones, F. C., Lukasiak, A., Ptuskin, V., & Webber, W. 2001a, Proc. 27th Int. Cosmic-Ray Conf. (Hamburg), 1844
———. 2001b, ApJ, 547, 264
Knie, K., Korschinek, G., Faestermann, T., Wallner, C., Scholten, J., & Hillebrandt, W. 1999, Phys. Rev. Lett., 83, 18
Leske, R. A. 1993, ApJ, 405, 567
Lukasiak, A., McDonald, F. B., & Webber, W. R. 1997, ApJ, 488, 454
———. 1999, Proc. 26th Int. Cosmic-Ray Conf. (Salt Lake City), 3, 41
Maíz-Apellániz, J. 2001, ApJ, 560, L83
Mashnik, S. G., Sierk, A. J., Van Riper, K. A., & Wilson, W. B. 1998, in Proc. Fourth Workshop on Simulating Accelerator Radiation Environments, ed. T. A. Gabriel (Oak Ridge, TN: ORNL), 151
Maurin, D., Donato, F., Taillet, R., & Salati, P. 2001, ApJ, 555, 585
Menn, W., et al. 2000, ApJ, 533, 281
Meyer, J.-P., Drury, L. O'C., & Ellison, D. C. 1998, Space Sci. Rev., 86, 179
Mitchell, J. W., et al. 1996, Phys. Rev. Lett., 76, 3057
Molnar, A., & Simon, M. 2001, Proc. 27th Int. Cosmic-Ray Conf. (Hamburg), 1877
Morfill, G. E., & Freyberg, M. J. 1998, in IAU Colloq. 166, The Local Bubble and Beyond, ed. D. Breitschwerdt, M. J. Freyberg, & J. Trümper (LNP 506; Berlin: Springer), 177
Moskalenko, I. V., Mashnik, S. G., & Strong, A. W. 2001a, Proc. 27th Int. Cosmic-Ray Conf. (Hamburg), 1836
Moskalenko, I. V., Strong, A. W., Ormes, J. F., & Potgieter, M. S. 2002, ApJ, 565, 280
Moskalenko, I. V., Strong, A. W., Ormes, J. F., Potgieter, M. S., & Langner, U. W. 2001b, Proc. 27th Int. Cosmic-Ray Conf. (Hamburg), 1868
Olson, D. L., Berman, B. L., Greiner, D. E., Heckman, H. H., Lindstrom, P. J., & Crawford, H. J. 1983, Phys. Rev. C, 28, 1602
Orito, S., et al. 2000, Phys. Rev. Lett., 84, 1078
Ptuskin, V. S., & Soutoul, A. 1990, A&A, 237, 445
Sanuki, T., et al. 2000, ApJ, 545, 1135
Savage, C., Apponi, A. J., Ziurys, L. M., & Wycoff, S. 2002, ApJ, 578, 211
Seo, E. S., Ormes, J. F., Streitmatter, R. E., Stochaj, S. J., Jones, W. V., Stephens, S. A., & Bowen, T. 1991, ApJ, 378, 763
Sfeir, D. M., Lallement, R., Crifo, F., & Welsh, B. Y. 1999, A&A, 346, 785
Silberberg, R., Tsao, C. H., & Barghouty, A. F. 1998, ApJ, 501, 911
Simpson, J. A., & Connell, J. J. 1998, ApJ, 497, L85
Sonett, C. P., Morfill, G. E., & Jokipii, J. R. 1987, Nature, 330, 458
Stephens, S. A., & Streitmatter, R. E. 1998, ApJ, 505, 266
Strong, A. W., & Moskalenko, I. V. 1998, ApJ, 509, 212
———. 2001, Adv. Space Res., 27, 717
Strong, A. W., Moskalenko, I. V., & Reimer, O. 2000, ApJ, 537, 763 (erratum 541, 1109)
Van Riper, K. A., Mashnik, S. G., & Wilson, W. B. 2001, Nucl. Instrum. Methods Phys. Res. A, 463, 576
Webber, W. R., Kish, J. C., Rockstroh, J. M., Cassagnou, Y., Legrain, R., Soutoul, A., Testard, O., & Tull, C. 1998a, ApJ, 508, 949
Webber, W. R., Kish, J. C., & Schrier, D. A. 1990a, Phys. Rev. C, 41, 547
———. 1990b, Phys. Rev. C, 41, 566
Webber, W. R., Lukasiak, A., & McDonald, F. B. 1997, ApJ, 476, 766
Webber, W. R., Lukasiak, A., McDonald, F. B., & Ferrando, P. 1996, ApJ, 457, 435
Webber, W. R., Soutoul, A., Kish, J. C., Rockstroh, J. M., Cassagnou, Y., Legrain, R., & Testard, O. 1998b, Phys. Rev. C, 58, 3539
Wiedenbeck, M. E., et al. 2001, Space Sci. Rev., 99, 15
Wuosmaa, A. H., et al. 1998, Phys. Rev. Lett., 80, 2085